J. Phys. B: At. Mol. Opt. Phys. **33** (2000) 4389–4408. Printed in the UK PII: S0953-4075(00)15436-7

Electron-impact excitation of Ne^{4+}

D C Griffin† and N R Badnell‡

† Department of Physics, Rollins College, Winter Park, FL 32789, USA
‡ Department of Physics and Applied Physics, University of Strathclyde, Glasgow G4 0NG, UK

Received 11 July 2000, in final form 18 August 2000

Abstract. We present the results of extensive close-coupling calculations of electron-impact excitation of the C-like ion, Ne^{4+}. We first compare effective collision strengths determined from a 20-level Breit–Pauli R-matrix calculation with those obtained from a 20-level intermediate-coupling frame transformation (ICFT) R-matrix calculation. The ICFT method was also employed to perform two much larger calculations; we compare the effective collision strengths determined from these calculations with each other and with those obtained from the 20-level calculations in order to assess the effects of increasing both the size of the configuration-interaction expansion of the target and the size of the close-coupling expansion. Our final calculation, with 130 terms and 261 levels in the configuration-interaction expansion of the target and 66 terms and 138 levels in the close-coupling expansion, provides improved data for excitation between the levels of the $2s^22p^2$, $2s2p^3$ and $2p^4$ configurations and the first close-coupling results for excitation to the levels of the $2s^22p3\ell$ configurations in Ne^{4+}.

1. Introduction

Accurate radiative and electron-collisional data for the ions of Ne are of significant importance to the diagnostics of astrophysical and laboratory plasmas. C-like Ne^{4+} is one of the more abundant ions of Ne and lines from this ion have been observed, for example, in planetary and gaseous nebula as well as in the solar corona. Also, Ne is used to cool the impurity plasma in the divertor chamber of a magnetic fusion tokomak. In this paper, we report on a series of R-matrix close-coupling calculations of the effective collision strengths for the electron-impact excitation of Ne^{4+}. There have been a number of earlier R-matrix calculations of electron-impact excitation in this ion [1–7]. However, in these prior studies, the close-coupling expansions were restricted to the 12 terms from the configurations $2s^22p^2$, $2s2p^3$, and $2p^4$. In addition, all these calculations were performed in LS coupling, although Aggarwal [5] and later Lennon and Burke [6, 7] determined effective collision strengths between individual levels by transforming their LS scattering matrices to pure pair coupling.

We began our work on Ne^{4+} by performing a Breit–Pauli (BP) R-matrix calculation in which we included only the 20 levels arising from the $2s^22p^2$, $2s2p^3$ and $2p^4$ configurations. We then repeated this calculation using the recently developed intermediate-coupling frame transformation (ICFT) method [8]. It is based on the application of multi-channel quantum-defect theory. We first generate unphysical K-matrices in pure LS coupling. These matrices are then transformed to intermediate coupling using term-coupling coefficients. Finally, the physical K-matrices are determined from the unphysical K-matrices and level energies using standard quantum-defect theory. This method has been shown [8] to avoid the problems associated with the transformation of the physical K-matrices to intermediate coupling in the

0953-4075/00/204389+20$30.00

presence of closed-channels, as is often done using the program JAJOM [10]. Furthermore, the ICFT method allows one to determine collision strengths between individual intermediate-coupled levels that are in excellent agreement with a full BP calculation, but in far less time [9].

Here we have provided additional evidence of the accuracy of the ICFT method by comparing the 20-level ICFT effective collision strengths with those obtained from our 20-level BP calculation. We then carried out two much larger ICFT R-matrix calculations. The first of these included the 34 terms and 62 levels within the $2s^22p^2$, $2s2p^3$, $2p^4$, $2s^22p3s$, $2s^22p3p$, $2s^22p3d$ and $2s2p^23s$ configurations. The second included the 48 terms and 88 levels within the $2s^22p^2$, $2s2p^3$, $2p^4$, $2s^22p3s$, $2s^22p3p$, $2s^22p3d$, $2s2p^23s$, $2s^22p4s$, $2s^22p4p$ and $2s^22p4d$ configurations, plus the lowest 18 terms and 50 levels from the $2s2p^23p$ and $2s2p^23d$ configurations, for a total of 66 terms and 138 levels. The effective collision strengths determined from these two calculations are compared with each other and with the two 20-level calculations in order to assess the cumulative effects of a more complete description of the target, the addition of more resonance contributions as higher levels are added to the calculation and the increase in level coupling as the size of the close-coupling expansion is increased. The electric-dipole radiative rates and effective collision strengths resulting from the largest of these calculations have been made available on the internet at the Oak Ridge National Laboratory (ORNL) Controlled Fusion Atomic Data Center (CFADC)†.

The remainder of this paper is organized as follows. In section 2, we describe our structure and scattering calculations for this ion and present some of our results for energies, radiative rates and effective collision strengths. In section 3, we summarize our findings.

2. Description of theoretical calculations

2.1. Bound-state calculations

The bound-state radial wavefunctions for all scattering calculations that were included in this work were determined using Froese Fischer's multi-configuration Hartree–Fock (MCHF) program [11]. The 1s, 2s and 2p orbitals that were employed for the BP 20-level R-matrix calculation and the 12-term, 20-level ICFT R-matrix calculation were determined from a single-configuration Hartree–Fock calculation on the $2s^22p^2\ ^3P$ term. This set of orbitals was then employed in Breit–Pauli configuration-interaction calculations that included the 10 even-parity levels arising from the configurations $2s^22p^2$ and $2p^4$, and the 10 odd-parity levels arising from the configuration $2s2p^3$. This resulted in the energies given in table 1 in comparison with the experimental values [12]. This set of orbitals does not provide a very complete description of the target, and if we were only interested in 20-level R-matrix calculations, we would want to supplement the configuration-interaction expansion with configurations involving the 3ℓ orbitals. However, our 20-level calculations were done primarily to provide an additional test of the accuracy of the ICFT method, and a larger configuration-interaction expansion would not have added to this.

For our 34-term, 62-level ICFT R-matrix calculation, we added 3s, 3p and 3d orbitals to the 1s, 2s and 2p orbitals, described above. The 3s orbital was generated by minimizing the energy of the $2s^22p3s\ ^3P$ term in an MCHF calculation that included the $2s^22p3s\ ^3P$ and $2p^33s\ ^3P$ terms. The 3p orbital was determined by minimizing the energy of the $2s^22p3p\ ^3D$ term in an MCHF calculation that included the $2s^22p3p\ ^3D$ and $2p^33p\ ^3D$ terms. Finally, the 3d orbital was determined by minimizing the energy of the $2s^22p3d\ ^3F$ term in an MCHF calculation that included the $2s^22p3d\ ^3F$ and $2p^33d\ ^3F$ terms. These orbitals were then employed in Breit–Pauli

† http://www-cfadc.phy.ornl.gov/data_and_codes

Table 1. Energies in eV for the levels included in the 20-level BP and ICFT *R*-matrix calculations for Ne^{4+} relative to the $2s^22p^2\ ^3P_0$ ground level.

Level	Energy (theory)	Energy (expt[a])	Level	Energy (theory)	Energy (expt[a])
$2s^22p^2\ ^3P_0$	0.00	0.00	$2s^22p^2\ ^3P_1$	0.05	0.05
$2s^22p^2\ ^3P_2$	0.13	0.14	$2s^22p^2\ ^1D_2$	4.10	3.76
$2s^22p^2\ ^1S_0$	7.67	7.92	$2s2p^3\ ^5S_2$	9.69	10.96
$2s2p^3\ ^3D_3$	22.46	21.80	$2s2p^3\ ^3D_2$	22.47	21.81
$2s2p^3\ ^3D_1$	22.48	21.81	$2s2p^3\ ^3P_2$	26.48	25.81
$2s2p^3\ ^3P_1$	26.48	25.81	$2s2p^3\ ^3P_0$	26.49	25.81
$2s2p^3\ ^1D_2$	36.00	33.55	$2s2p^3\ ^3S_1$	36.75	34.64
$2s2p^3\ ^1P_1$	40.00	37.67	$2p^4\ ^3P_2$	53.62	51.17
$2p^4\ ^3P_1$	53.72	51.26	$2p^4\ ^3P_0$	53.77	51.31
$2p^4\ ^1D_2$	57.68	—	$2p^4\ ^1S_0$	66.15	—

[a] Kelly [12].

configuration-interaction calculations that included the 64 even-parity levels arising from the $2s^22p^2$, $2p^4$, $2s^22p3p$, $2s2p^23s$ and $2p^33p$ configurations and the 73 odd-parity levels arising from the $2s2p^3$, $2s^22p3s$, $2s^22p3d$, $2p^33s$ and $2p^33d$ configurations. The energies resulting from this calculation for the 62 levels included in the ICFT calculation are shown in comparison with the experimental values [12] in table 2.

For our 66-term, 138-level ICFT *R*-matrix calculation, we added the 4s, 4p and 4d orbitals to the 1s, 2s, 2p, 3s, 3p and 3d orbitals. The 4s orbital was determined from a single-configuration Hartree–Fock calculation on the $2s^22p4s\ ^3P$ term; the 4p orbital was determined from a single-configuration Hartree–Fock calculation on the $2s^22p4p\ ^3D$ term; and the 4d orbital was determined from a single-configuration Hartree–Fock calculation on the $2s^22p4d\ ^3F$ term. These orbitals were then employed in Breit–Pauli configuration-interaction calculations that involved the 130 even-parity levels arising from the configurations $2s^22p^2$, $2p^4$, $2s^22p3p$, $2s2p^23s$, $2s2p^23d$, $2s^22p4p$ and $2p^33p$ and the 131 odd-parity levels arising from the configurations $2s2p^3$, $2s^22p3s$, $2s^22p3d$, $2s2p^23p$, $2s^22p4s$, $2s^22p4d$, $2p^33s$ and $2p^33d$. The energies that resulted from these calculations for the 138 levels included in our final ICFT calculation are shown in comparison with the experimental values [12] in table 3. In table 4, we also show the electric-dipole radiative rates that resulted from this large bound-state calculation for selected transitions to the levels of the $2s^22p^2$ configuration; they are compared with the radiative rates for this ion calculated by Aggarwal [13], using the program CIV3. Our radiative rates are also plotted against those of Aggarwal [13] in figure 1. As can be seen from table 4 and figure 1, the agreement between these two sets of radiative rates is, in general, very good; there are some rates that differ more significantly, but those are confined almost entirely to the weaker transitions.

2.2. Scattering calculations

In this section, we describe a series of *R*-matrix calculations of effective collision strengths in Ne^{4+}. The effective collision strength, Υ, first introduced by Seaton [14], is defined by the equation

$$\Upsilon_{ij} = \int_0^\infty \Omega(i \to j) \exp\left(\frac{-\epsilon_j}{kT_e}\right) \mathrm{d}\left(\frac{\epsilon_j}{kT_e}\right) \tag{1}$$

Table 2. Energies in eV for the levels included in the 62-level ICFT R-matrix calculation for Ne^{4+} relative to the $2s^22p^2\ ^3P_0$ ground level.

Level	Energy (theory)	Energy (expt[a])	Level	Energy (theory)	Energy (expt[a])
$2s^22p^2\ ^3P_0$	0.00	0.00	$2s^22p^2\ ^3P_1$	0.05	0.05
$2s^22p^2\ ^3P_2$	0.13	0.14	$2s^22p^2\ ^1D_2$	4.15	3.76
$2s^22p^2\ ^1S_0$	7.64	7.92	$2s2p^3\ ^5S_2$	9.73	10.96
$2s2p^3\ ^3D_3$	22.16	21.80	$2s2p^3\ ^3D_2$	22.17	21.81
$2s2p^3\ ^3D_1$	22.17	21.81	$2s2p^3\ ^3P_2$	26.32	25.81
$2s2p^3\ ^3P_1$	26.32	25.81	$2s2p^3\ ^3P_0$	26.32	25.81
$2s2p^3\ ^1D_2$	35.28	33.55	$2s2p^3\ ^3S_1$	36.08	34.64
$2s2p^3\ ^1P_1$	39.50	37.67	$2p^4\ ^3P_2$	53.37	51.17
$2p^4\ ^3P_1$	53.47	51.26	$2p^4\ ^3P_0$	53.51	51.31
$2p^4\ ^1D_2$	57.38	—	$2p^4\ ^1S_0$	65.46	—
$2s^22p3s\ ^3P_0$	74.20	73.93	$2s^22p3s\ ^3P_1$	74.24	73.97
$2s^22p3s\ ^3P_2$	74.34	74.08	$2s^22p3s\ ^1P_1$	75.56	75.04
$2s^22p3p\ ^1P_1$	78.73	78.78	$2s^22p3p\ ^3D_1$	79.34	79.40
$2s^22p3p\ ^3D_2$	79.40	79.46	$2s^22p3p\ ^3D_3$	79.48	79.55
$2s^22p3p\ ^3S_1$	80.09	80.14	$2s^22p3p\ ^3P_0$	80.79	80.68
$2s^22p3p\ ^3P_1$	80.83	80.73	$2s^22p3p\ ^3P_2$	80.88	80.79
$2s^22p3p\ ^1D_2$	83.02	82.26	$2s^22p3p\ ^1S_0$	85.32	84.12
$2s2p^23s\ ^5P_1$	85.67	86.42	$2s2p^23s\ ^5P_2$	85.72	86.49
$2s^22p3d\ ^3F_2$	85.73	85.55	$2s^22p3d\ ^3F_3$	85.79	85.66
$2s2p^23s\ ^5P_3$	85.79	86.54	$2s^22p3d\ ^3F_4$	85.86	85.74
$2s^22p3d\ ^1D_2$	85.97	85.63	$2s^22p3d\ ^3D_1$	87.08	86.57
$2s^22p3d\ ^3D_2$	87.10	86.59	$2s^22p3d\ ^3D_3$	87.13	86.63
$2s^22p3d\ ^3P_2$	87.42	87.01	$2s^22p3d\ ^3P_1$	87.46	87.05
$2s^22p3d\ ^3P_0$	87.48	87.09	$2s^22p3d\ ^1P_1$	89.10	87.09
$2s^22p3d\ ^1F_3$	89.10	88.02	$2s2p^23s\ ^3P_0$	89.68	89.19
$2s2p^23s\ ^3P_1$	89.72	89.21	$2s2p^23s\ ^3P_2$	89.79	89.27
$2s2p^23s\ ^3D_3$	97.17	96.46	$2s2p^23s\ ^3D_2$	97.17	—
$2s2p^23s\ ^3D_1$	97.17	—	$2s2p^23s\ ^1D_2$	99.49	—
$2s2p^23s\ ^3S_1$	103.36	—	$2s2p^23s\ ^1S_0$	105.58	—
$2s2p^23s\ ^3P_0$	106.51	—	$2s2p^23s\ ^3P_1$	106.53	—
$2s2p^23s\ ^3P_2$	106.59	—	$2s2p^23s\ ^1P_1$	107.57	—

[a] Kelly [12].

where Ω is the collision strength for the transition from level i to level j and ϵ_j is the continuum energy of the final scattered electron. Effective collision strengths have a much more gradual variation with temperature than rate coefficients and are, therefore, much better suited for interpolation over temperature. We employed the integration technique of Burgess and Tully [15] to calculate the effective collision strengths.

Our R-matrix calculations were based on a modified version of the RMATRIX I atomic scattering package [16]. We first performed a 20-level BP R-matrix calculation in which the 20 levels listed in table 1 were included in the close-coupling expansion. For this calculation, the size of the R-matrix box was 3.8 au and we used 15 basis orbitals to represent the continuum for each value of the orbital angular momentum. We performed a BP calculation with exchange for all $J\Pi$ partial waves from $J = 0.5$ to 9.5. In the resonance region, we made calculations at 5305 energy points with an energy mesh spacing of 9.2×10^{-4} Ryd, while in the energy region above the highest threshold, we made calculations at an additional 101 points with a

Table 3. Energies in eV for the levels included in the 138-level ICFT *R*-matrix calculation for Ne^{4+} relative to the $2s^22p^2\ ^3P_0$ ground level.

Level	Energy (theory)	Energy (expt[a])	Level	Energy (theory)	Energy (expt[a])
$2s^22p^2\ ^3P_0$	0.00	0.00	$2s^22p^2\ ^3P_1$	0.05	0.05
$2s^22p^2\ ^3P_2$	0.13	0.14	$2s^22p^2\ ^1D_2$	4.13	3.76
$2s^22p^2\ ^1S_0$	7.97	7.92	$2s2p^3\ ^5S_2$	10.07	10.96
$2s2p^3\ ^3D_3$	22.36	21.80	$2s2p^3\ ^3D_2$	22.37	21.81
$2s2p^3\ ^3D_1$	22.37	21.81	$2s2p^3\ ^3P_2$	26.45	25.81
$2s2p^3\ ^3P_1$	26.46	25.81	$2s2p^3\ ^3P_0$	26.46	25.81
$2s2p^3\ ^1D_2$	35.43	33.55	$2s2p^3\ ^3S_1$	36.35	34.64
$2s2p^3\ ^1P_1$	39.60	37.67	$2p^4\ ^3P_2$	53.12	51.17
$2p^4\ ^3P_1$	53.21	51.26	$2p^4\ ^3P_0$	53.26	51.31
$2p^4\ ^1D_2$	56.79	—	$2p^4\ ^1S_0$	65.15	—
$2s^22p3s\ ^3P_0$	73.99	73.93	$2s^22p3s\ ^3P_1$	74.03	73.97
$2s^22p3s\ ^3P_2$	74.13	74.08	$2s^22p3s\ ^1P_1$	75.46	75.04
$2s^22p3p\ ^1P_1$	78.95	78.78	$2s^22p3p\ ^3D_1$	79.53	79.40
$2s^22p3p\ ^3D_2$	79.59	79.46	$2s^22p3p\ ^3D_3$	79.67	79.55
$2s^22p3p\ ^3S_1$	80.36	80.14	$2s^22p3p\ ^3P_0$	80.98	80.68
$2s^22p3p\ ^3P_1$	81.02	80.73	$2s^22p3p\ ^3P_2$	81.07	80.79
$2s^22p3p\ ^1D_2$	83.07	82.26	$2s^22p3p\ ^1S_0$	85.16	84.12
$2s2p^23s\ ^5P_1$	85.96	86.42	$2s^22p3d\ ^3F_2$	85.97	85.55
$2s2p^23s\ ^5P_2$	86.01	86.49	$2s^22p3d\ ^3F_3$	86.03	85.66
$2s2p^23s\ ^5P_3$	86.07	86.54	$2s^22p3d\ ^3F_4$	86.10	85.74
$2s^22p3d\ ^1D_2$	86.14	85.63	$2s^22p3d\ ^3D_1$	87.20	86.57
$2s^22p3d\ ^3D_2$	87.22	86.59	$2s^22p3d\ ^3D_3$	87.25	86.63
$2s^22p3d\ ^3P_2$	87.53	87.01	$2s^22p3d\ ^3P_1$	87.57	87.05
$2s^22p3d\ ^3P_0$	87.59	87.09	$2s^22p3d\ ^1P_1$	89.08	87.09
$2s^22p3d\ ^1F_3$	89.13	88.02	$2s2p^23s\ ^3P_0$	89.84	89.19
$2s2p^23s\ ^3P_1$	89.88	89.21	$2s2p^23s\ ^3P_2$	89.95	89.27
$2s2p^23p\ ^3S_1$	91.04	91.40	$2s2p^23p\ ^5D_0$	91.54	—
$2s2p^23p\ ^5D_1$	91.55	91.96	$2s2p^23p\ ^5D_2$	91.58	92.00
$2s2p^23p\ ^5D_3$	91.62	92.05	$2s2p^23p\ ^5D_4$	91.68	92.11
$2s2p^23p\ ^5P_1$	92.18	—	$2s2p^23p\ ^5P_2$	92.20	—
$2s2p^23p\ ^5P_3$	92.25	—	$2s2p^23p\ ^3D_1$	94.23	—
$2s2p^23p\ ^3D_2$	94.27	93.99	$2s2p^23p\ ^3D_3$	94.32	94.04
$2s2p^23p\ ^5S_2$	94.72	—	$2s2p^23p\ ^3P_0$	95.42	94.90
$2s2p^23p\ ^3P_1$	95.43	94.93	$2s2p^23p\ ^3P_2$	95.45	94.97
$2s2p^23s\ ^3D_1$	97.32	—	$2s2p^23s\ ^3D_2$	97.32	—
$2s2p^23s\ ^3D_3$	97.32	96.46	$2s2p^23d\ ^5F_1$	97.41	—
$2s2p^23d\ ^5F_2$	97.42	—	$2s2p^23d\ ^5F_3$	97.44	—
$2s2p^23d\ ^5F_4$	97.48	—	$2s2p^23d\ ^5F_5$	97.51	—
$2s2p^23d\ ^5D_0$	98.20	—	$2s2p^23d\ ^5D_1$	98.21	—
$2s2p^23d\ ^5D_2$	98.21	—	$2s2p^23d\ ^5D_3$	98.22	98.61
$2s2p^23d\ ^5D_4$	98.24	—	$2s2p^23d\ ^5P_3$	98.97	99.02
$2s2p^23d\ ^5P_2$	99.00	99.04	$2s2p^23d\ ^5P_1$	99.02	99.06
$2s2p^23d\ ^3P_2$	99.56	99.29	$2s2p^23d\ ^3P_1$	99.60	99.35
$2s2p^23s\ ^1D_2$	99.61	—	$2s2p^23d\ ^3P_0$	99.63	99.38
$2s2p^23d\ ^3F_2$	100.41	99.88	$2s2p^23d\ ^3F_3$	100.45	99.92
$2s2p^23d\ ^3F_4$	100.50	99.98	$2s^22p4s\ ^3P_0$	101.41	98.60
$2s^22p4s\ ^3P_1$	101.45	98.60	$2s^22p4s\ ^3P_2$	101.55	98.60
$2s^22p4s\ ^1P_1$	101.99	99.84	$2s2p^23d\ ^3D_1$	102.06	—
$2s2p^23d\ ^3D_2$	102.07	101.19	$2s2p^23d\ ^3D_3$	102.09	101.21

Table 3. Continued.

Level	Energy (theory)	Energy (expt[a])	Level	Energy (theory)	Energy (expt[a])
$2s2p^2 3s\ ^3S_1$	103.00	—	$2s2p^2 3p\ ^3F_2$	103.10	—
$2s2p^2 3p\ ^3F_3$	103.11	—	$2s2p^2 3p\ ^3F_4$	103.13	—
$2s^2 2p4p\ ^1P_1$	103.32	—	$2s2p^2 3p\ ^1D_2$	103.34	—
$2s^2 2p4p\ ^3D_1$	103.87	—	$2s^2 2p4p\ ^3D_2$	103.91	—
$2s^2 2p4p\ ^3D_3$	104.00	—	$2s2p^2 3p\ ^1F_3$	104.00	102.30
$2s2p^2 3p\ ^3D_1$	104.32	—	$2s2p^2 3p\ ^3D_2$	104.32	—
$2s2p^2 3p\ ^3D_3$	104.33	—	$2s^2 2p4p\ ^3P_0$	104.42	—
$2s^2 2p4p\ ^3P_1$	104.44	—	$2s^2 2p4p\ ^3P_2$	104.51	—
$2s^2 2p4p\ ^3S_1$	104.56	—	$2s2p^2 3p\ ^1P_1$	104.76	—
$2s2p^2 3s\ ^1S_0$	104.95	—	$2s^2 2p4p\ ^1D_2$	105.17	—
$2s2p^2 3p\ ^3P_2$	105.63	—	$2s2p^2 3p\ ^3P_1$	105.64	—
$2s2p^2 3p\ ^3P_0$	105.64	—	$2s^2 2p4d\ ^3F_2$	106.03	—
$2s^2 2p4d\ ^3F_3$	106.09	—	$2s^2 2p4d\ ^3F_4$	106.16	—
$2s^2 2p4d\ ^1D_2$	106.18	103.98	$2s^2 2p4d\ ^3D_1$	106.55	104.40
$2s^2 2p4d\ ^3D_2$	106.57	104.40	$2s^2 2p4p\ ^1S_0$	106.58	—
$2s^2 2p4d\ ^3D_3$	106.61	104.40	$2s^2 2p4d\ ^3P_2$	106.72	104.51
$2s^2 2p4d\ ^3P_1$	106.75	104.51	$2s^2 2p4d\ ^3P_0$	106.77	104.51
$2s2p^2 3s\ ^3P_0$	106.89	—	$2s2p^2 3s\ ^3P_1$	106.92	—
$2s2p^2 3s\ ^3P_2$	106.98	—	$2s^2 2p4d\ ^1P_1$	107.42	—
$2s^2 2p4d\ ^1F_3$	107.55	104.95	$2s2p^2 3s\ ^1P_1$	108.20	—

[a] Kelly [12].

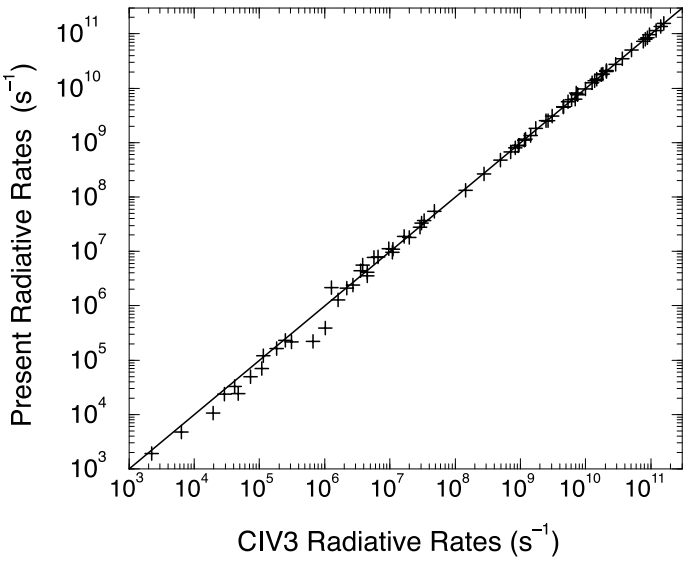

Figure 1. Graphical comparison of the radiative rates given in table 4.

mesh spacing of 0.102 Ryd; this allowed us to calculate collision strengths up to an energy of 15 Ryd, which is sufficiently high to determine effective collision strengths up to a temperature of 1.0×10^6 K.

Table 4. Ne^{4+} electric-dipole radiative rates for selected transitions to the levels of the $2s^22p^2$ configuration.

Transition	Present[a]	CIV3[b]
$2s2p^3\ ^3D_1$–$2s^22p^2\ ^3P_0$	7.11×10^8	6.70×10^8
$2s2p^3\ ^3P_1$–$2s^22p^2\ ^3P_0$	1.15×10^9	1.10×10^9
$2s2p^3\ ^3S_1$–$2s^22p^2\ ^3P_0$	2.48×10^9	2.52×10^9
$2s2p^3\ ^1P_1$–$2s^22p^2\ ^3P_0$	7.27×10^4	5.00×10^4
$2s^22p3s\ ^3P_1$–$2s^22p^2\ ^3P_0$	6.08×10^9	6.09×10^9
$2s^22p3s\ ^1P_1$–$2s^22p^2\ ^3P_0$	5.66×10^6	7.71×10^6
$2s^22p3d\ ^3D_1$–$2s^22p^2\ ^3P_0$	8.87×10^{10}	8.49×10^{10}
$2s^22p3d\ ^3P_1$–$2s^22p^2\ ^3P_0$	1.75×10^{10}	1.79×10^{10}
$2s^22p3d\ ^1P_1$–$2s^22p^2\ ^3P_0$	4.82×10^7	5.45×10^7
$2s2p^3\ ^5S_2$–$2s^22p^2\ ^3P_1$	2.23×10^3	1.90×10^3
$2s2p^3\ ^3D_2$–$2s^22p^2\ ^3P_1$	9.52×10^8	8.97×10^8
$2s2p^3\ ^3D_1$–$2s^22p^2\ ^3P_1$	4.97×10^8	4.72×10^8
$2s2p^3\ ^3P_2$–$2s^22p^2\ ^3P_1$	8.31×10^8	7.94×10^8
$2s2p^3\ ^3P_1$–$2s^22p^2\ ^3P_1$	9.24×10^8	8.80×10^8
$2s2p^3\ ^1D_2$–$2s^22p^2\ ^3P_1$	1.14×10^5	1.20×10^5
$2s2p^3\ ^3S_1$–$2s^22p^2\ ^3P_1$	7.44×10^9	7.57×10^9
$2s2p^3\ ^1P_1$–$2s^22p^2\ ^3P_1$	4.54×10^6	3.58×10^6
$2s^22p3s\ ^3P_0$–$2s^22p^2\ ^3P_1$	1.83×10^{10}	1.83×10^{10}
$2s^22p3s\ ^3P_1$–$2s^22p^2\ ^3P_1$	4.55×10^9	4.55×10^9
$2s^22p3s\ ^3P_2$–$2s^22p^2\ ^3P_1$	4.57×10^9	4.58×10^9
$2s^22p3s\ ^1P_1$–$2s^22p^2\ ^3P_1$	9.69×10^6	1.12×10^7
$2s^22p3d\ ^3D_1$–$2s^22p^2\ ^3P_1$	5.09×10^{10}	4.99×10^{10}
$2s^22p3d\ ^3D_2$–$2s^22p^2\ ^3P_1$	1.20×10^{11}	1.14×10^{11}
$2s^22p3d\ ^3P_2$–$2s^22p^2\ ^3P_1$	7.21×10^9	8.10×10^9
$2s^22p3d\ ^3P_1$–$2s^22p^2\ ^3P_1$	2.89×10^{10}	2.73×10^{10}
$2s^22p3d\ ^1P_1$–$2s^22p^2\ ^3P_1$	1.98×10^7	1.82×10^7
$2s^22p3d\ ^3P_0$–$2s^22p^2\ ^3P_1$	8.22×10^{10}	7.98×10^{10}
$2s2p^3\ ^5S_2$–$2s^22p^2\ ^3P_2$	6.38×10^3	4.78×10^3
$2s2p^3\ ^3D_3$–$2s^22p^2\ ^3P_2$	1.21×10^9	1.15×10^9
$2s2p^3\ ^3D_2$–$2s^22p^2\ ^3P_2$	2.76×10^8	2.64×10^8
$2s2p^3\ ^3D_1$–$2s^22p^2\ ^3P_2$	2.88×10^7	2.78×10^7
$2s2p^3\ ^3P_2$–$2s^22p^2\ ^3P_2$	2.66×10^9	2.53×10^9
$2s2p^3\ ^3P_1$–$2s^22p^2\ ^3P_2$	1.43×10^9	1.36×10^9
$2s2p^3\ ^1D_2$–$2s^22p^2\ ^3P_2$	2.17×10^6	2.13×10^6
$2s2p^3\ ^3S_1$–$2s^22p^2\ ^3P_2$	1.25×10^{10}	1.27×10^{10}
$2s2p^3\ ^1P_1$–$2s^22p^2\ ^3P_2$	6.62×10^5	2.19×10^5
$2s^22p3s\ ^3P_1$–$2s^22p^2\ ^3P_2$	7.65×10^9	7.64×10^9
$2s^22p3s\ ^3P_2$–$2s^22p^2\ ^3P_2$	1.37×10^{10}	1.37×10^{10}
$2s^22p3s\ ^1P_1$–$2s^22p^2\ ^3P_2$	3.55×10^6	4.40×10^6
$2s^22p3d\ ^3D_1$–$2s^22p^2\ ^3P_2$	1.73×10^9	1.83×10^9
$2s^22p3d\ ^3D_2$–$2s^22p^2\ ^3P_2$	2.07×10^{10}	2.12×10^{10}
$2s^22p3d\ ^3D_3$–$2s^22p^2\ ^3P_2$	1.42×10^{11}	1.37×10^{11}
$2s^22p3d\ ^3P_2$–$2s^22p^2\ ^3P_2$	7.63×10^{10}	7.26×10^{10}
$2s^22p3d\ ^3P_1$–$2s^22p^2\ ^3P_2$	3.63×10^{10}	3.51×10^{10}
$2s^22p3d\ ^1P_1$–$2s^22p^2\ ^3P_2$	1.60×10^6	1.29×10^6
$2s^22p3d\ ^1F_3$–$2s^22p^2\ ^3P_2$	1.27×10^6	2.15×10^6
$2s2p^3\ ^3D_3$–$2s^22p^2\ ^1D_2$	1.83×10^5	1.65×10^5
$2s2p^3\ ^3D_2$–$2s^22p^2\ ^1D_2$	4.20×10^4	3.29×10^4
$2s2p^3\ ^3D_1$–$2s^22p^2\ ^1D_2$	2.91×10^4	2.38×10^4
$2s2p^3\ ^3P_2$–$2s^22p^2\ ^1D_2$	4.78×10^4	2.45×10^4

Table 4. Continued.

Transition	Present[a]	CIV3[b]
$2s2p^3\ ^3P_1–2s^22p^2\ ^1D_2$	2.50×10^5	2.29×10^5
$2s2p^3\ ^1D_2–2s^22p^2\ ^1D_2$	1.00×10^{10}	9.78×10^9
$2s2p^3\ ^3S_1–2s^22p^2\ ^1D_2$	1.02×10^6	3.85×10^5
$2s2p^3\ ^1P_1–2s^22p^2\ ^1D_2$	1.47×10^{10}	1.46×10^{10}
$2s^22p3s\ ^3P_1–2s^22p^2\ ^1D_2$	3.08×10^7	3.29×10^7
$2s^22p3s\ ^3P_2–2s^22p^2\ ^1D_2$	4.47×10^6	4.13×10^6
$2s^22p3s\ ^1P_1–2s^22p^2\ ^1D_2$	2.08×10^{10}	2.01×10^{10}
$2s^22p3d\ ^3D_1–2s^22p^2\ ^1D_2$	1.11×10^7	1.10×10^7
$2s^22p3d\ ^3D_2–2s^22p^2\ ^1D_2$	1.01×10^7	9.67×10^6
$2s^22p3d\ ^3D_3–2s^22p^2\ ^1D_2$	3.81×10^6	5.60×10^6
$2s^22p3d\ ^3P_2–2s^22p^2\ ^1D_2$	1.44×10^8	1.33×10^8
$2s^22p3d\ ^3P_1–2s^22p^2\ ^1D_2$	2.74×10^6	2.38×10^6
$2s^22p3d\ ^1P_1–2s^22p^2\ ^1D_2$	5.35×10^9	5.65×10^9
$2s^22p3d\ ^1F_3–2s^22p^2\ ^1D_2$	1.59×10^{11}	1.56×10^{11}
$2s2p^3\ ^3D_1–2s^22p^2\ ^1S_0$	1.97×10^4	1.06×10^4
$2s2p^3\ ^3P_1–2s^22p^2\ ^1S_0$	1.09×10^5	6.96×10^4
$2s2p^3\ ^3S_1–2s^22p^2\ ^1S_0$	3.10×10^5	2.16×10^5
$2s2p^3\ ^1P_1–2s^22p^2\ ^1S_0$	3.07×10^9	3.06×10^9
$2s^22p3s\ ^3P_1–2s^22p^2\ ^1S_0$	6.58×10^6	7.87×10^6
$2s^22p3s\ ^1P_1–2s^22p^2\ ^1S_0$	6.94×10^9	6.34×10^9
$2s^22p3d\ ^3D_1–2s^22p^2\ ^1S_0$	3.32×10^7	3.72×10^7
$2s^22p3d\ ^3P_1–2s^22p^2\ ^1S_0$	1.66×10^7	1.87×10^7
$2s^22p3d\ ^1P_1–2s^22p^2\ ^1S_0$	9.52×10^{10}	9.60×10^{10}

[a] Calculated using the same configuration-interaction basis states that were employed to determine the energies in table 3.
[b] Aggarwal [13].

An expansion in $J\Pi$ partial waves up to $J = 9.5$ is not sufficiently complete for the determination of collision strengths up to an energy of 15 Ryd. In order to complete the sum, we employed the no-exchange R-matrix codes [17] to perform R-matrix calculations in LS coupling without exchange for all $LS\Pi$ partial waves from $L = 8$ to 40 and generated unphysical K-matrices in LS coupling. These were then transformed to intermediate coupling using our ICFT method; this allowed us to determine physical K-matrices up to a total J value of 37.5. These high-J contributions were then topped-up as follows: the dipole transitions were topped-up using a method originally described by Burgess [18] for LS coupling and implemented here in intermediate coupling; the non-dipole transitions were topped-up assuming a geometric series in J, using energy ratios, and with a special procedure to handle transitions between nearly degenerate levels based on the degenerate limiting case [19]†. It is also important to note that, in the asymptotic region, we included the long-range multipole potentials perturbatively for all partial waves. Finally, in order to increase the accuracy of the scattering calculations, the target energies were adjusted to their experimental values, where known.

† In a recent article, Aggarwal *et al* [20] showed that there were some problems with our earlier calculations on Fe^{14+} [9]. These were primarily due to a long-standing error in the no-exchange codes that we have now corrected. In addition, at certain energies there were problems in the high partial-wave collision strengths for a few transitions that caused problems in our top-up procedure. These difficulties have also been eliminated in the latest versions of our programs. In addition, the high-partial wave, no-exchange portions of all prior calculations that employed these methods have been repeated and the data at the ORNL CFADC internet site have been updated.

Table 5. Ne^{4+} effective collision strengths for selected transitions between the levels of the $2s^2 2p^2$ configuration. For each transition, the first row is from Lennon and Burke [7]; the second row is from the present 20-level BP calculation; the third row is from the present 12-term, 20-level ICFT calculation; the fourth row is from the present 34-term, 62-level ICFT calculation; and the fifth row is from the present 66-term, 138-level ICFT calculation.

	Electron temperature (K)						
Transition	1.00×10^3	2.51×10^3	6.30×10^3	1.00×10^4	2.51×10^4	6.30×10^4	1.00×10^5
$^3P_0$–$^3P_1$	1.83×10^0	1.82×10^0	1.61×10^0	1.41×10^0	1.01×10^0	7.88×10^{-1}	7.16×10^{-1}
	2.43×10^0	2.21×10^0	1.91×10^0	1.67×10^0	1.18×10^0	9.11×10^{-1}	8.23×10^{-1}
	2.71×10^0	2.34×10^0	1.96×10^0	1.70×10^0	1.19×10^0	9.21×10^{-1}	8.34×10^{-1}
	2.25×10^0	2.16×10^0	1.89×10^0	1.65×10^0	1.16×10^0	8.87×10^{-1}	8.01×10^{-1}
	2.59×10^0	2.32×10^0	1.90×10^0	1.61×10^0	1.10×10^0	8.28×10^{-1}	7.46×10^{-1}
$^3P_0$–$^3P_2$	3.23×10^0	2.98×10^0	2.24×10^0	1.81×10^0	1.10×10^0	7.21×10^{-1}	6.10×10^{-1}
	3.14×10^0	2.82×10^0	2.16×10^0	1.78×10^0	1.11×10^0	7.51×10^{-1}	6.45×10^{-1}
	3.13×10^0	2.80×10^0	2.16×10^0	1.77×10^0	1.11×10^0	7.50×10^{-1}	6.42×10^{-1}
	3.00×10^0	2.97×10^0	2.33×10^0	1.91×10^0	1.17×10^0	7.61×10^{-1}	6.44×10^{-1}
	3.05×10^0	2.74×10^0	2.01×10^0	1.62×10^0	9.75×10^{-1}	6.46×10^{-1}	5.54×10^{-1}
$^3P_0$–$^1D_2$	1.99×10^{-1}	2.35×10^{-1}	2.35×10^{-1}	2.32×10^{-1}	2.42×10^{-1}	2.42×10^{-1}	2.30×10^{-1}
	1.44×10^{-1}	1.92×10^{-1}	2.14×10^{-1}	2.21×10^{-1}	2.51×10^{-1}	2.58×10^{-1}	2.44×10^{-1}
	1.41×10^{-1}	1.89×10^{-1}	2.12×10^{-1}	2.19×10^{-1}	2.50×10^{-1}	2.58×10^{-1}	2.44×10^{-1}
	1.48×10^{-1}	1.91×10^{-1}	1.98×10^{-1}	1.98×10^{-1}	2.10×10^{-1}	2.19×10^{-1}	2.12×10^{-1}
	1.57×10^{-1}	2.05×10^{-1}	2.10×10^{-1}	2.06×10^{-1}	2.10×10^{-1}	2.14×10^{-1}	2.06×10^{-1}
$^3P_0$–$^1S_0$	3.55×10^{-2}	3.07×10^{-2}	2.77×10^{-2}	2.73×10^{-2}	2.82×10^{-2}	2.82×10^{-2}	2.72×10^{-2}
	4.25×10^{-2}	3.62×10^{-2}	2.98×10^{-2}	2.84×10^{-2}	2.85×10^{-2}	2.81×10^{-2}	2.69×10^{-2}
	4.33×10^{-2}	3.72×10^{-2}	3.05×10^{-2}	2.89×10^{-2}	2.88×10^{-2}	2.83×10^{-2}	2.71×10^{-2}
	4.21×10^{-2}	3.99×10^{-2}	3.27×10^{-2}	3.03×10^{-2}	2.89×10^{-2}	2.83×10^{-2}	2.71×10^{-2}
	5.38×10^{-2}	4.47×10^{-2}	3.53×10^{-2}	3.18×10^{-2}	2.87×10^{-2}	2.76×10^{-2}	2.65×10^{-2}
$^3P_1$–$^3P_2$	9.55×10^0	8.98×10^0	7.04×10^0	5.83×10^0	3.72×10^0	2.60×10^0	2.25×10^0
	9.23×10^0	8.69×10^0	7.08×10^0	5.96×10^0	3.90×10^0	2.81×10^0	2.47×10^0
	9.18×10^0	8.65×10^0	7.05×10^0	5.94×10^0	3.89×10^0	2.80×10^0	2.46×10^0
	9.24×10^0	9.19×10^0	7.49×10^0	6.27×10^0	4.02×10^0	2.79×10^0	2.44×10^0
	9.35×10^0	8.64×10^0	6.65×10^0	5.47×10^0	3.47×10^0	2.45×10^0	2.16×10^0
$^3P_1$–$^1D_2$	5.96×10^{-1}	7.06×10^{-1}	7.05×10^{-1}	6.96×10^{-1}	7.26×10^{-1}	7.26×10^{-1}	6.90×10^{-1}
	4.38×10^{-1}	5.83×10^{-1}	6.47×10^{-1}	6.67×10^{-1}	7.57×10^{-1}	7.79×10^{-1}	7.38×10^{-1}
	4.32×10^{-1}	5.75×10^{-1}	6.41×10^{-1}	6.62×10^{-1}	7.54×10^{-1}	7.77×10^{-1}	7.36×10^{-1}
	4.52×10^{-1}	5.80×10^{-1}	5.99×10^{-1}	5.98×10^{-1}	6.34×10^{-1}	6.60×10^{-1}	6.42×10^{-1}
	4.76×10^{-1}	6.18×10^{-1}	6.35×10^{-1}	6.21×10^{-1}	6.34×10^{-1}	6.46×10^{-1}	6.23×10^{-1}
$^3P_1$–$^1S_0$	1.07×10^{-1}	9.21×10^{-2}	8.31×10^{-2}	8.19×10^{-2}	8.46×10^{-2}	8.46×10^{-2}	8.16×10^{-2}
	1.26×10^{-1}	1.07×10^{-1}	8.92×10^{-2}	8.53×10^{-2}	8.64×10^{-2}	8.56×10^{-2}	8.22×10^{-2}
	1.28×10^{-1}	1.10×10^{-1}	9.07×10^{-2}	8.64×10^{-2}	8.73×10^{-2}	8.66×10^{-2}	8.31×10^{-2}
	1.27×10^{-1}	1.20×10^{-1}	9.84×10^{-2}	9.14×10^{-2}	8.73×10^{-2}	8.58×10^{-2}	8.26×10^{-2}
	1.61×10^{-1}	1.34×10^{-1}	1.06×10^{-1}	9.59×10^{-2}	8.70×10^{-2}	8.38×10^{-2}	8.07×10^{-2}
$^3P_2$–$^1D_2$	9.93×10^{-1}	1.18×10^0	1.18×10^0	1.16×10^0	1.21×10^0	1.21×10^0	1.15×10^0
	7.66×10^{-1}	1.01×10^0	1.10×10^0	1.13×10^0	1.27×10^0	1.30×10^0	1.24×10^0
	7.55×10^{-1}	9.95×10^{-1}	1.09×10^0	1.12×10^0	1.26×10^0	1.30×10^0	1.23×10^0
	7.93×10^{-1}	1.00×10^0	1.02×10^0	1.02×10^0	1.07×10^0	1.11×10^0	1.07×10^0
	8.05×10^{-1}	1.04×10^0	1.07×10^0	1.05×10^0	1.07×10^0	1.09×10^0	1.05×10^0

Table 5. Continued.

	Electron temperature (K)						
Transition	1.00×10^3	2.51×10^3	6.30×10^3	1.00×10^4	2.51×10^4	6.30×10^4	1.00×10^5
$^3P_2$–$^1S_0$	1.78×10^{-1}	1.54×10^{-1}	1.39×10^{-1}	1.37×10^{-1}	1.41×10^{-1}	1.41×10^{-1}	1.36×10^{-1}
	1.98×10^{-1}	1.70×10^{-1}	1.45×10^{-1}	1.41×10^{-1}	1.45×10^{-1}	1.45×10^{-1}	1.39×10^{-1}
	2.01×10^{-1}	1.73×10^{-1}	1.47×10^{-1}	1.42×10^{-1}	1.46×10^{-1}	1.45×10^{-1}	1.39×10^{-1}
	2.09×10^{-1}	1.96×10^{-1}	1.63×10^{-1}	1.52×10^{-1}	1.46×10^{-1}	1.44×10^{-1}	1.38×10^{-1}
	2.68×10^{-1}	2.25×10^{-1}	1.79×10^{-1}	1.62×10^{-1}	1.46×10^{-1}	1.40×10^{-1}	1.35×10^{-1}

So as to provide a further test of the ICFT method, which is used for the two largest calculations in this study, we repeated the above calculation using the ICFT method for all partial waves. The specifics for this 12-term, 20-level ICFT calculation were similar to those given above for the 20-level BP calculation. The only difference is that we first performed a 12-term R-matrix calculation in LS coupling and then used the ICFT method to generate physical K-matrices for all $J\Pi$ partial waves from $J = 0.5$ to 9.5. The high-$J\Pi$ partial-wave contributions with top-up were determined from the no-exchange calculation described above.

In table 5, we compare the effective collision strengths calculated with our 20-level BP calculation (row 2) and our 12-term, 20-level ICFT calculation (row 3) for selected transitions among the levels of the $2s^22p^2$ configuration. These may also be compared with the effective collision strengths resulting from the calculations of Lennon and Burke [7] shown in row 1. We see that the BP and ICFT results are in excellent agreement. In fact, the average difference between the two sets of effective collision strengths given in the second and third rows in table 5 for all transitions is only 1.2%. On the other hand, the agreement between the results of the present 20-level calculations and those of Lennon and Burke [7] is less satisfactory, especially at low temperatures. For example, the average difference between the effective collision strengths of Lennon and Burke and those from the present BP calculation is 10.9%. Beyond the differences in target orbitals, the primary difference between these calculations is that Lennon and Burke determined their collision strengths between levels by transforming their LS coupling scattering matrices to pure pair coupling, while both our BP and ICFT calculations yield collision strengths in intermediate coupling.

In table 6, we present the effective collision strengths determined from the present 20-level BP calculation (row 1) and the present 12-term, 20-level ICFT calculation (row 2) for excitations from the three levels of the $2s^22p^2\ ^3P$ ground term to the ten levels of the $2s2p^3$ configuration. Again the agreement between these two calculations is excellent with an average difference of only 0.9%. However, both sets of 20-level effective collision strengths are suspect due to the fact that they employ a very limited configuration-interaction expansion of the target and do not include resonant contributions from higher levels or coupling to such levels. The coupling effects should reduce these effective collision strengths, while the resonant contributions should increase them.

In order to improve on the effective collision strengths for transitions among the levels of the $2s^22p^2$, $2s2p^3$ and $2p^4$ configurations and to include excitation to the levels of the $2s^22p3\ell$ configurations, we undertook much larger R-matrix calculations. However, due to the fact that full BP calculations are very time consuming when a large number of levels is included in the close-coupling expansion, and in light of the accuracy of the ICFT method, we carried out these larger calculations using only the ICFT method.

We first performed an ICFT R-matrix calculation that included the 34 terms arising from the $2s^22p^2$, $2s2p^3$, $2p^4$, $2s^22p3s$, $2s^22p3p$, $2s^22p3d$ and $2s2p^23s$ configurations in the LS-

Table 6. Ne^{4+} effective collision strengths for the transitions from the levels of the $2s^2 2p^2\ ^3P$ term to the levels of the $2s2p^3$ configuration. For each transition, the first row is from the present 20-level BP calculation; the second row is from the present 12-term, 20-level ICFT calculation; the third row is from the present 34-term, 62-level ICFT calculation; and the fourth row is from the present 66-term, 138-level ICFT calculation.

	Electron temperature (K)						
Transition	1.00×10^4	2.51×10^4	6.30×10^4	1.00×10^5	2.51×10^5	6.30×10^5	1.00×10^6
$^3P_0$–$^5S_2$	1.67×10^{-1}	1.55×10^{-1}	1.28×10^{-1}	1.12×10^{-1}	7.76×10^{-2}	5.10×10^{-2}	4.07×10^{-2}
	1.65×10^{-1}	1.53×10^{-1}	1.28×10^{-1}	1.11×10^{-1}	7.77×10^{-2}	5.11×10^{-2}	4.08×10^{-2}
	1.61×10^{-1}	1.46×10^{-1}	1.19×10^{-1}	1.03×10^{-1}	7.21×10^{-2}	4.89×10^{-2}	3.95×10^{-2}
	1.40×10^{-1}	1.38×10^{-1}	1.16×10^{-1}	1.02×10^{-1}	7.22×10^{-2}	4.93×10^{-2}	3.98×10^{-2}
$^3P_0$–$^3D_3$	5.99×10^{-2}	7.92×10^{-2}	6.86×10^{-2}	5.56×10^{-2}	3.14×10^{-2}	1.58×10^{-2}	1.09×10^{-2}
	6.16×10^{-2}	8.21×10^{-2}	7.12×10^{-2}	5.77×10^{-2}	3.25×10^{-2}	1.63×10^{-2}	1.12×10^{-2}
	1.18×10^{-1}	9.62×10^{-2}	7.15×10^{-2}	5.69×10^{-2}	3.24×10^{-2}	1.68×10^{-2}	1.18×10^{-2}
	1.06×10^{-1}	8.65×10^{-2}	6.63×10^{-2}	5.32×10^{-2}	3.11×10^{-2}	1.72×10^{-2}	1.23×10^{-2}
$^3P_0$–$^3D_2$	5.17×10^{-2}	6.24×10^{-2}	5.82×10^{-2}	5.18×10^{-2}	3.83×10^{-2}	2.72×10^{-2}	2.24×10^{-2}
	5.19×10^{-2}	6.33×10^{-2}	5.91×10^{-2}	5.25×10^{-2}	3.86×10^{-2}	2.73×10^{-2}	2.25×10^{-2}
	6.91×10^{-2}	6.56×10^{-2}	5.77×10^{-2}	5.19×10^{-2}	4.11×10^{-2}	3.08×10^{-2}	2.56×10^{-2}
	8.15×10^{-2}	7.17×10^{-2}	6.10×10^{-2}	5.43×10^{-2}	4.35×10^{-2}	3.36×10^{-2}	2.80×10^{-2}
$^3P_0$–$^3D_1$	6.61×10^{-1}	6.70×10^{-1}	6.78×10^{-1}	6.91×10^{-1}	7.37×10^{-1}	8.30×10^{-1}	9.01×10^{-1}
	6.63×10^{-1}	6.71×10^{-1}	6.78×10^{-1}	6.91×10^{-1}	7.36×10^{-1}	8.30×10^{-1}	9.01×10^{-1}
	5.88×10^{-1}	6.00×10^{-1}	6.09×10^{-1}	6.21×10^{-1}	6.64×10^{-1}	7.47×10^{-1}	8.11×10^{-1}
	5.65×10^{-1}	5.70×10^{-1}	5.76×10^{-1}	5.86×10^{-1}	6.27×10^{-1}	7.06×10^{-1}	7.65×10^{-1}
$^3P_0$–$^3P_2$	2.85×10^{-2}	2.36×10^{-2}	1.92×10^{-2}	1.68×10^{-2}	1.24×10^{-2}	8.54×10^{-3}	6.92×10^{-3}
	2.76×10^{-2}	2.30×10^{-2}	1.90×10^{-2}	1.68×10^{-2}	1.24×10^{-2}	8.56×10^{-3}	6.93×10^{-3}
	2.82×10^{-2}	2.78×10^{-2}	2.37×10^{-2}	2.12×10^{-2}	1.70×10^{-2}	1.23×10^{-2}	9.87×10^{-3}
	3.75×10^{-2}	3.03×10^{-2}	2.32×10^{-2}	2.03×10^{-2}	1.73×10^{-2}	1.36×10^{-2}	1.11×10^{-2}
$^3P_0$–$^3P_1$	5.17×10^{-1}	5.43×10^{-1}	5.67×10^{-1}	5.84×10^{-1}	6.32×10^{-1}	7.19×10^{-1}	7.84×10^{-1}
	5.08×10^{-1}	5.37×10^{-1}	5.65×10^{-1}	5.83×10^{-1}	6.31×10^{-1}	7.19×10^{-1}	7.84×10^{-1}
	5.00×10^{-1}	5.18×10^{-1}	5.39×10^{-1}	5.57×10^{-1}	6.06×10^{-1}	6.91×10^{-1}	7.58×10^{-1}
	4.56×10^{-1}	4.66×10^{-1}	4.84×10^{-1}	5.00×10^{-1}	5.43×10^{-1}	6.19×10^{-1}	6.74×10^{-1}
$^3P_0$–$^3P_0$	7.87×10^{-3}	7.30×10^{-3}	6.67×10^{-3}	6.27×10^{-3}	5.31×10^{-3}	4.18×10^{-3}	3.56×10^{-3}
	7.57×10^{-3}	7.10×10^{-3}	6.58×10^{-3}	6.20×10^{-3}	5.29×10^{-3}	4.18×10^{-3}	3.56×10^{-3}
	7.97×10^{-3}	7.48×10^{-3}	7.08×10^{-3}	6.95×10^{-3}	6.64×10^{-3}	5.44×10^{-3}	4.59×10^{-3}
	9.40×10^{-3}	8.10×10^{-3}	7.18×10^{-3}	6.86×10^{-3}	6.52×10^{-3}	5.47×10^{-3}	4.64×10^{-3}
$^3P_0$–$^1D_2$	3.28×10^{-2}	2.75×10^{-2}	2.33×10^{-2}	2.18×10^{-2}	1.89×10^{-2}	1.55×10^{-2}	1.35×10^{-2}
	3.28×10^{-2}	2.75×10^{-2}	2.33×10^{-2}	2.18×10^{-2}	1.89×10^{-2}	1.55×10^{-2}	1.35×10^{-2}
	3.45×10^{-2}	2.95×10^{-2}	2.60×10^{-2}	2.52×10^{-2}	2.38×10^{-2}	1.98×10^{-2}	1.69×10^{-2}
	3.49×10^{-2}	3.00×10^{-2}	2.62×10^{-2}	2.50×10^{-2}	2.34×10^{-2}	1.97×10^{-2}	1.69×10^{-2}
$^3P_0$–$^3S_1$	3.80×10^{-1}	3.83×10^{-1}	3.88×10^{-1}	3.97×10^{-1}	4.27×10^{-1}	4.89×10^{-1}	5.37×10^{-1}
	3.82×10^{-1}	3.85×10^{-1}	3.90×10^{-1}	3.98×10^{-1}	4.28×10^{-1}	4.90×10^{-1}	5.37×10^{-1}
	3.86×10^{-1}	3.89×10^{-1}	3.94×10^{-1}	4.03×10^{-1}	4.31×10^{-1}	4.93×10^{-1}	5.49×10^{-1}
	3.88×10^{-1}	3.91×10^{-1}	3.95×10^{-1}	4.02×10^{-1}	4.27×10^{-1}	4.83×10^{-1}	5.20×10^{-1}
$^3P_0$–$^1P_1$	8.26×10^{-3}	8.45×10^{-3}	8.44×10^{-3}	8.27×10^{-3}	7.56×10^{-3}	6.28×10^{-3}	5.44×10^{-3}
	8.27×10^{-3}	8.45×10^{-3}	8.44×10^{-3}	8.28×10^{-3}	7.56×10^{-3}	6.28×10^{-3}	5.44×10^{-3}
	1.03×10^{-2}	1.12×10^{-2}	1.17×10^{-2}	1.19×10^{-2}	1.17×10^{-2}	9.51×10^{-3}	8.29×10^{-3}
	1.03×10^{-2}	1.07×10^{-2}	1.09×10^{-2}	1.09×10^{-2}	1.06×10^{-2}	8.68×10^{-3}	7.19×10^{-3}

Table 6. Continued.

	Electron temperature (K)						
Transition	1.00×10^4	2.51×10^4	6.30×10^4	1.00×10^5	2.51×10^5	6.30×10^5	1.00×10^6
$^3P_1$–$^5S_2$	5.05×10^{-1}	4.67×10^{-1}	3.86×10^{-1}	3.36×10^{-1}	2.33×10^{-1}	1.53×10^{-1}	1.22×10^{-1}
	4.99×10^{-1}	4.60×10^{-1}	3.78×10^{-1}	3.29×10^{-1}	2.29×10^{-1}	1.51×10^{-1}	1.21×10^{-1}
	4.82×10^{-1}	4.33×10^{-1}	3.49×10^{-1}	3.02×10^{-1}	2.13×10^{-1}	1.45×10^{-1}	1.18×10^{-1}
	4.22×10^{-1}	4.15×10^{-1}	3.49×10^{-1}	3.06×10^{-1}	2.17×10^{-1}	1.48×10^{-1}	1.18×10^{-1}
$^3P_1$–$^3D_3$	1.93×10^{-1}	2.46×10^{-1}	2.19×10^{-1}	1.84×10^{-1}	1.16×10^{-1}	6.95×10^{-2}	5.30×10^{-2}
	1.98×10^{-1}	2.55×10^{-1}	2.26×10^{-1}	1.89×10^{-1}	1.19×10^{-1}	7.05×10^{-2}	5.37×10^{-2}
	3.68×10^{-1}	3.05×10^{-1}	2.33×10^{-1}	1.92×10^{-1}	1.25×10^{-1}	7.77×10^{-2}	5.99×10^{-2}
	3.30×10^{-1}	2.78×10^{-1}	2.22×10^{-1}	1.85×10^{-1}	1.24×10^{-1}	8.18×10^{-2}	6.40×10^{-2}
$^3P_1$–$^3D_2$	1.60×10^{0}	1.65×10^{0}	1.64×10^{0}	1.65×10^{0}	1.71×10^{0}	1.90×10^{0}	2.05×10^{0}
	1.60×10^{0}	1.65×10^{0}	1.64×10^{0}	1.65×10^{0}	1.71×10^{0}	1.90×10^{0}	2.05×10^{0}
	1.49×10^{0}	1.50×10^{0}	1.48×10^{0}	1.49×10^{0}	1.55×10^{0}	1.71×10^{0}	1.85×10^{0}
	1.43×10^{0}	1.43×10^{0}	1.41×10^{0}	1.41×10^{0}	1.46×10^{0}	1.62×10^{0}	1.74×10^{0}
$^3P_1$–$^3D_1$	5.43×10^{-1}	5.61×10^{-1}	5.59×10^{-1}	5.58×10^{-1}	5.72×10^{-1}	6.22×10^{-1}	6.66×10^{-1}
	5.44×10^{-1}	5.62×10^{-1}	5.60×10^{-1}	5.59×10^{-1}	5.73×10^{-1}	6.23×10^{-1}	6.66×10^{-1}
	5.11×10^{-1}	5.16×10^{-1}	5.11×10^{-1}	5.11×10^{-1}	5.26×10^{-1}	5.70×10^{-1}	6.08×10^{-1}
	5.14×10^{-1}	5.04×10^{-1}	4.92×10^{-1}	4.90×10^{-1}	5.04×10^{-1}	5.46×10^{-1}	5.78×10^{-1}
$^3P_1$–$^3P_2$	6.90×10^{-1}	7.10×10^{-1}	7.29×10^{-1}	7.45×10^{-1}	7.91×10^{-1}	8.87×10^{-1}	9.61×10^{-1}
	6.75×10^{-1}	7.00×10^{-1}	7.25×10^{-1}	7.42×10^{-1}	7.90×10^{-1}	8.87×10^{-1}	9.61×10^{-1}
	6.68×10^{-1}	6.90×10^{-1}	7.06×10^{-1}	7.22×10^{-1}	7.73×10^{-1}	8.65×10^{-1}	9.39×10^{-1}
	6.35×10^{-1}	6.32×10^{-1}	6.38×10^{-1}	6.50×10^{-1}	6.95×10^{-1}	7.78×10^{-1}	8.38×10^{-1}
$^3P_1$–$^3P_1$	4.63×10^{-1}	4.79×10^{-1}	4.93×10^{-1}	5.04×10^{-1}	5.36×10^{-1}	6.00×10^{-1}	6.50×10^{-1}
	4.54×10^{-1}	4.73×10^{-1}	4.91×10^{-1}	5.03×10^{-1}	5.36×10^{-1}	6.00×10^{-1}	6.50×10^{-1}
	4.47×10^{-1}	4.61×10^{-1}	4.74×10^{-1}	4.86×10^{-1}	5.22×10^{-1}	5.83×10^{-1}	6.33×10^{-1}
	4.24×10^{-1}	4.23×10^{-1}	4.30×10^{-1}	4.39×10^{-1}	4.71×10^{-1}	5.26×10^{-1}	5.65×10^{-1}
$^3P_1$–$^3P_0$	5.31×10^{-1}	5.56×10^{-1}	5.81×10^{-1}	5.99×10^{-1}	6.47×10^{-1}	7.37×10^{-1}	8.03×10^{-1}
	5.23×10^{-1}	5.52×10^{-1}	5.79×10^{-1}	5.98×10^{-1}	6.48×10^{-1}	7.38×10^{-1}	8.04×10^{-1}
	5.15×10^{-1}	5.32×10^{-1}	5.53×10^{-1}	5.70×10^{-1}	6.20×10^{-1}	7.07×10^{-1}	7.75×10^{-1}
	4.70×10^{-1}	4.79×10^{-1}	4.96×10^{-1}	5.12×10^{-1}	5.56×10^{-1}	6.33×10^{-1}	6.90×10^{-1}
$^3P_1$–$^1D_2$	9.94×10^{-2}	8.33×10^{-2}	7.06×10^{-2}	6.59×10^{-2}	5.72×10^{-2}	4.68×10^{-2}	4.05×10^{-2}
	9.93×10^{-2}	8.32×10^{-2}	7.05×10^{-2}	6.58×10^{-2}	5.71×10^{-2}	4.68×10^{-2}	4.04×10^{-2}
	1.04×10^{-1}	8.91×10^{-2}	7.86×10^{-2}	7.62×10^{-2}	7.24×10^{-2}	6.06×10^{-2}	5.34×10^{-2}
	1.05×10^{-1}	9.06×10^{-2}	7.90×10^{-2}	7.55×10^{-2}	7.07×10^{-2}	5.91×10^{-2}	4.97×10^{-2}
$^3P_1$–$^3S_1$	1.15×10^{0}	1.16×10^{0}	1.17×10^{0}	1.20×10^{0}	1.29×10^{0}	1.48×10^{0}	1.62×10^{0}
	1.15×10^{0}	1.16×10^{0}	1.17×10^{0}	1.20×10^{0}	1.29×10^{0}	1.48×10^{0}	1.62×10^{0}
	1.16×10^{0}	1.17×10^{0}	1.19×10^{0}	1.21×10^{0}	1.30×10^{0}	1.49×10^{0}	1.66×10^{0}
	1.17×10^{0}	1.18×10^{0}	1.19×10^{0}	1.21×10^{0}	1.29×10^{0}	1.46×10^{0}	1.57×10^{0}
$^3P_1$–$^1P_1$	2.58×10^{-2}	2.64×10^{-2}	2.64×10^{-2}	2.59×10^{-2}	2.38×10^{-2}	2.00×10^{-2}	1.75×10^{-2}
	2.59×10^{-2}	2.65×10^{-2}	2.64×10^{-2}	2.60×10^{-2}	2.38×10^{-2}	2.00×10^{-2}	1.75×10^{-2}
	3.18×10^{-2}	3.46×10^{-2}	3.61×10^{-2}	3.69×10^{-2}	3.64×10^{-2}	2.97×10^{-2}	2.60×10^{-2}
	3.21×10^{-2}	3.33×10^{-2}	3.37×10^{-2}	3.39×10^{-2}	3.28×10^{-2}	2.69×10^{-2}	2.24×10^{-2}

Table 6. Continued.

	Electron temperature (K)						
Transition	1.00×10^4	2.51×10^4	6.30×10^4	1.00×10^5	2.51×10^5	6.30×10^5	1.00×10^6
$^3P_2$–$^5S_2$	8.63×10^{-1}	7.93×10^{-1}	6.60×10^{-1}	5.77×10^{-1}	4.00×10^{-1}	2.61×10^{-1}	2.07×10^{-1}
	8.50×10^{-1}	7.79×10^{-1}	6.44×10^{-1}	5.63×10^{-1}	3.91×10^{-1}	2.57×10^{-1}	2.04×10^{-1}
	8.09×10^{-1}	7.26×10^{-1}	5.96×10^{-1}	5.20×10^{-1}	3.67×10^{-1}	2.48×10^{-1}	2.02×10^{-1}
	7.15×10^{-1}	7.02×10^{-1}	5.93×10^{-1}	5.21×10^{-1}	3.71×10^{-1}	2.50×10^{-1}	1.99×10^{-1}
$^3P_2$–$^3D_3$	2.97×10^0	3.06×10^0	3.05×10^0	3.05×10^0	3.16×10^0	3.48×10^0	3.75×10^0
	2.98×10^0	3.07×10^0	3.05×10^0	3.06×10^0	3.16×10^0	3.48×10^0	3.75×10^0
	2.76×10^0	2.78×10^0	2.76×10^0	2.77×10^0	2.87×10^0	3.16×10^0	3.39×10^0
	2.73×10^0	2.70×10^0	2.65×10^0	2.65×10^0	2.74×10^0	3.00×10^0	3.22×10^0
$^3P_2$–$^3D_2$	7.05×10^{-1}	7.60×10^{-1}	7.17×10^{-1}	6.80×10^{-1}	6.26×10^{-1}	6.32×10^{-1}	6.59×10^{-1}
	7.10×10^{-1}	7.71×10^{-1}	7.26×10^{-1}	6.87×10^{-1}	6.31×10^{-1}	6.35×10^{-1}	6.61×10^{-1}
	7.94×10^{-1}	7.38×10^{-1}	6.67×10^{-1}	6.31×10^{-1}	5.84×10^{-1}	5.87×10^{-1}	6.09×10^{-1}
	7.79×10^{-1}	7.18×10^{-1}	6.47×10^{-1}	6.10×10^{-1}	5.65×10^{-1}	5.67×10^{-1}	5.84×10^{-1}
$^3P_2$–$^3D_1$	1.64×10^{-1}	2.03×10^{-1}	1.82×10^{-1}	1.56×10^{-1}	1.06×10^{-1}	7.53×10^{-2}	6.70×10^{-2}
	1.66×10^{-1}	2.08×10^{-1}	1.86×10^{-1}	1.58×10^{-1}	1.07×10^{-1}	7.60×10^{-2}	6.74×10^{-2}
	3.04×10^{-1}	2.50×10^{-1}	1.91×10^{-1}	1.59×10^{-1}	1.08×10^{-1}	7.63×10^{-2}	6.69×10^{-2}
	2.53×10^{-1}	2.15×10^{-1}	1.74×10^{-1}	1.47×10^{-1}	1.03×10^{-1}	7.58×10^{-2}	6.63×10^{-2}
$^3P_2$–$^3P_2$	2.12×10^0	2.21×10^0	2.29×10^0	2.35×10^0	2.53×10^0	2.86×10^0	3.11×10^0
	2.08×10^0	2.18×10^0	2.28×10^0	2.35×10^0	2.53×10^0	2.86×10^0	3.10×10^0
	2.04×10^0	2.11×10^0	2.19×10^0	2.25×10^0	2.43×10^0	2.75×10^0	3.00×10^0
	1.90×10^0	1.92×10^0	1.97×10^0	2.03×10^0	2.19×10^0	2.47×10^0	2.68×10^0
$^3P_2$–$^3P_1$	7.12×10^{-1}	7.36×10^{-1}	7.61×10^{-1}	7.78×10^{-1}	8.29×10^{-1}	9.31×10^{-1}	1.01×10^0
	7.06×10^{-1}	7.34×10^{-1}	7.61×10^{-1}	7.79×10^{-1}	8.30×10^{-1}	9.32×10^{-1}	1.01×10^0
	6.99×10^{-1}	7.22×10^{-1}	7.38×10^{-1}	7.55×10^{-1}	8.06×10^{-1}	9.02×10^{-1}	9.79×10^{-1}
	6.63×10^{-1}	6.60×10^{-1}	6.67×10^{-1}	6.80×10^{-1}	7.26×10^{-1}	8.13×10^{-1}	8.76×10^{-1}
$^3P_2$–$^3P_0$	2.89×10^{-2}	2.43×10^{-2}	1.99×10^{-2}	1.75×10^{-2}	1.28×10^{-2}	8.84×10^{-3}	7.14×10^{-3}
	2.78×10^{-2}	2.35×10^{-2}	1.96×10^{-2}	1.73×10^{-2}	1.27×10^{-2}	8.80×10^{-3}	7.11×10^{-3}
	2.90×10^{-2}	2.92×10^{-2}	2.51×10^{-2}	2.25×10^{-2}	1.80×10^{-2}	1.29×10^{-2}	1.02×10^{-2}
	3.80×10^{-2}	3.08×10^{-2}	2.37×10^{-2}	2.08×10^{-2}	1.76×10^{-2}	1.37×10^{-2}	1.12×10^{-2}
$^3P_2$–$^1D_2$	1.68×10^{-1}	1.41×10^{-1}	1.19×10^{-1}	1.12×10^{-1}	9.69×10^{-2}	7.95×10^{-2}	6.89×10^{-2}
	1.68×10^{-1}	1.41×10^{-1}	1.19×10^{-1}	1.11×10^{-1}	9.67×10^{-2}	7.94×10^{-2}	6.88×10^{-2}
	1.76×10^{-1}	1.51×10^{-1}	1.33×10^{-1}	1.28×10^{-1}	1.21×10^{-1}	1.02×10^{-1}	8.98×10^{-2}
	1.77×10^{-1}	1.53×10^{-1}	1.33×10^{-1}	1.27×10^{-1}	1.19×10^{-1}	9.96×10^{-2}	8.39×10^{-2}
$^3P_2$–$^3S_1$	1.93×10^0	1.95×10^0	1.98×10^0	2.02×10^0	2.17×10^0	2.49×10^0	2.73×10^0
	1.94×10^0	1.96×10^0	1.98×10^0	2.03×10^0	2.18×10^0	2.49×10^0	2.74×10^0
	1.96×10^0	1.97×10^0	2.00×10^0	2.05×10^0	2.19×10^0	2.51×10^0	2.80×10^0
	1.97×10^0	1.99×10^0	2.01×10^0	2.04×10^0	2.17×10^0	2.45×10^0	2.64×10^0
$^3P_2$–$^1P_1$	4.43×10^{-2}	4.53×10^{-2}	4.52×10^{-2}	4.44×10^{-2}	4.07×10^{-2}	3.39×10^{-2}	2.94×10^{-2}
	4.43×10^{-2}	4.53×10^{-2}	4.53×10^{-2}	4.44×10^{-2}	4.07×10^{-2}	3.39×10^{-2}	2.94×10^{-2}
	5.47×10^{-2}	5.93×10^{-2}	6.21×10^{-2}	6.32×10^{-2}	6.16×10^{-2}	5.00×10^{-2}	4.37×10^{-2}
	5.50×10^{-2}	5.68×10^{-2}	5.73×10^{-2}	5.75×10^{-2}	5.53×10^{-2}	4.52×10^{-2}	3.75×10^{-2}

coupling portion of the calculation to finally produce intermediate-coupled collision strengths between the 62 levels listed in table 2. For this calculation, the size of the R-matrix box was 8.3 au. In our 20-level calculations, a basis set of 15 orbitals for each value of the angular momentum was larger than needed; however, here a basis set of this size was required to properly represent the continuum up to a maximum energy of 15 Ryd. In order to eliminate the resonances attached to the terms of the $2p^3 3s$, $2p^3 3p$ and $2p^3 3d$ configurations that were included in our configuration-interaction expansion of the target, but not our close-coupling expansion, we used the pseudo-resonance elimination method developed by Gorczyca *et al* [21]. As in the 12-term, 20-level ICFT calculation, we performed an LS R-matrix calculation with exchange for all $LS\Pi$ partial waves up to $L = 12$ to generate physical K-matrices with exchange from $J = 0.5$ to 9.5. We then again employed the no-exchange code to generate the high-$J\Pi$ partial waves up to $J = 37.5$ and topped-up. In the ICFT portion of the calculation, we had to eliminate the very weak mixing with levels arising from the terms included in the configuration-interaction expansion of the target, but not the close-coupling expansion, and renormalize the term-coupling coefficients. In the resonance region we made calculations at 8536 energy points with an energy mesh spacing of 9.2×10^{-4} Ryd; in the energy region above the highest threshold, we made calculations at an additional 101 points, with a mesh spacing of 0.071 Ryd and with the highest energy in the calculation at 15 Ryd. As in the 20-level calculations, the energies of the target were adjusted to the experimental values, where known.

The primary problem with the 34-term, 62-level calculation is that it does not include the contributions from resonances attached to the levels of the $2s^2 2p4\ell$ configurations nor the effects of coupling to these levels. It was for this reason that we performed one final calculation in our study of electron impact in Ne^{4+}. It included the 66 terms and the 138 levels listed in table 3. Here the size of the R-matrix box was 13.5 au and we employed 24 basis orbitals to represent the continuum for each value of the orbital angular momentum. We again used our pseudo-resonance elimination method to remove the resonances attached to all the terms of the $2p^3 3s$, $2p^3 3p$ and $2p^3 3d$ configurations and those terms of the $2s2p^2 3p$ and $2s2p^2 3d$ configurations that were not included in our close-coupling expansion. We also eliminated the weak mixing with the levels of these terms in the ICFT portion of the calculation. With the exception of the size of the calculation, the other specifics are the same as those described above for the 62-level calculation; however, we now had to carry out the calculation in the resonance region at 8638 points with the same energy spacing. With the 138 levels that we included here, a full BP calculation would have been prohibitively time consuming; however, we expect that it would have produced effective collision strengths in very close agreement with those determined from this ICFT calculation.

The effective collision strengths determined from the 62- and 138-level calculations are given in rows 4 and 5 in table 5 and in rows 3 and 4 in table 6. By comparing the 138- and 62-level results with each other and with the 20-level results, we see that the effective collision strengths for some transitions increase, while other decrease, as the size of the calculation is increased. Some of these differences are due to the improvement in the target states associated with the $2s^2 2p^2$, $2s2p^3$ and $2p^4$ configurations as the size of the configuration-interaction expansion is increased. However, they are also caused by the reductions arising from increased coupling between levels, the effects of which are impossible to distinguish from the increased configuration interaction, and enhancements arising from the increase in the resonant contributions. We illustrate this for three selected transitions between levels of $2s^2 2p^2$ and $2s2p^3$ in figures 2–4, where we compare collision strengths obtained from our four calculations. The results from our 20-level BP and ICFT calculations shown in frames (*a*) and (*b*) of these figures are seen to be nearly identical; this is typical of the other transitions for which we have compared the detailed collision strengths.

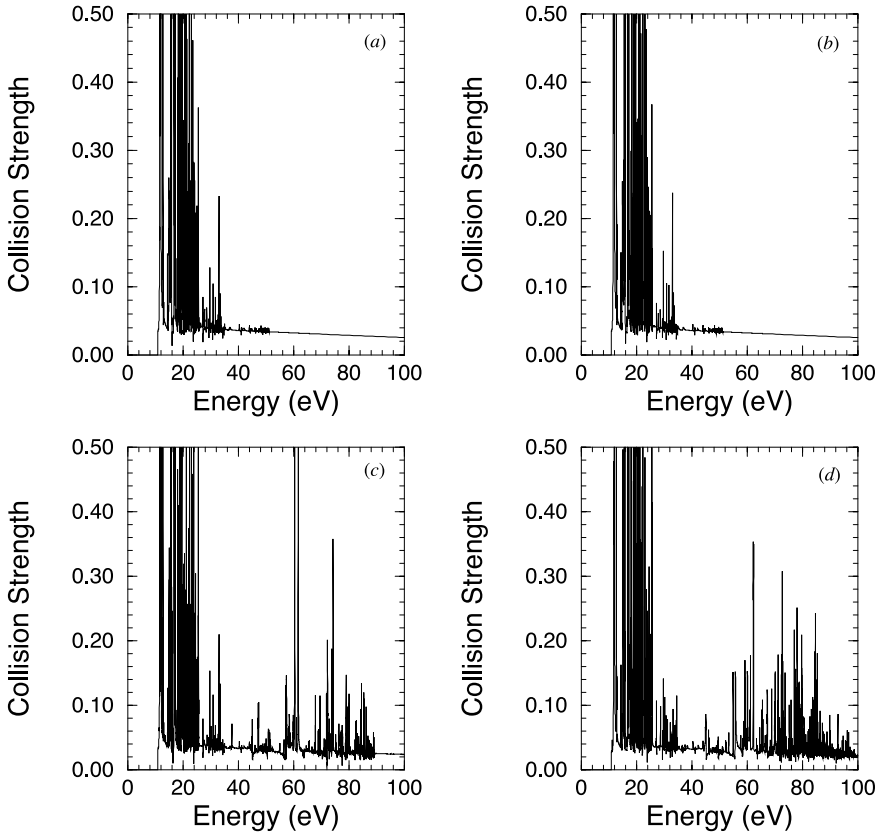

Figure 2. Collision strengths for excitation from $2s^22p^2\ ^3P_0$ to $2s2p^3\ ^5S_2$: (*a*) 20-level BP *R*-matrix calculation; (*b*) 20-level ICFT *R*-matrix calculation; (*c*) 62-level ICFT *R*-matrix calculation; (*d*) 138-level ICFT *R*-matrix calculation.

In figure 2, where we show the collision strengths for the $2s^22p^2\ ^3P_0$–$2s2p^3\ ^5S_2$ transition, there are additional resonance contributions from the higher levels included in the 62- and 138-level calculations that would tend to increase the effective collision strengths. However, the additional states included in the larger calculations also cause some small differences in the near-threshold resonance structure and small reductions in the background collision strengths; the overall effect for this transition is a reduction in the effective collision strengths. In figure 3, we compare our calculated collision strengths for the dipole-allowed $2s^22p^2\ ^3P_0$–$2s2p^3\ ^3D_1$ transition. Even though the two larger calculations include additional resonance contributions, the major effect is a reduction in the background collision strength arising from both the larger configuration-interaction expansion of the target and the additional coupling to higher levels. Finally, from figure 4, we see that the collision strength for the $2s^22p^2\ ^3P_1$–$2s2p^3\ ^3D_3$ transition is completely dominated by resonances; thus, it is the addition of the resonant contributions from the higher levels, included in the two larger calculations, that accounts for the increase in effective collision strengths for this transition.

We also compared our effective collision strengths given in table 6 with those of Aggarwal [5] and found significant differences, especially for the transitions between the levels of the $2s^22p^2\ ^3P$ ground term and the levels of the $2s2p^3\ ^3D$ and $2s2p^3\ ^3P$ terms. We would not have expected this level of discrepancy between these two calculations, even though the

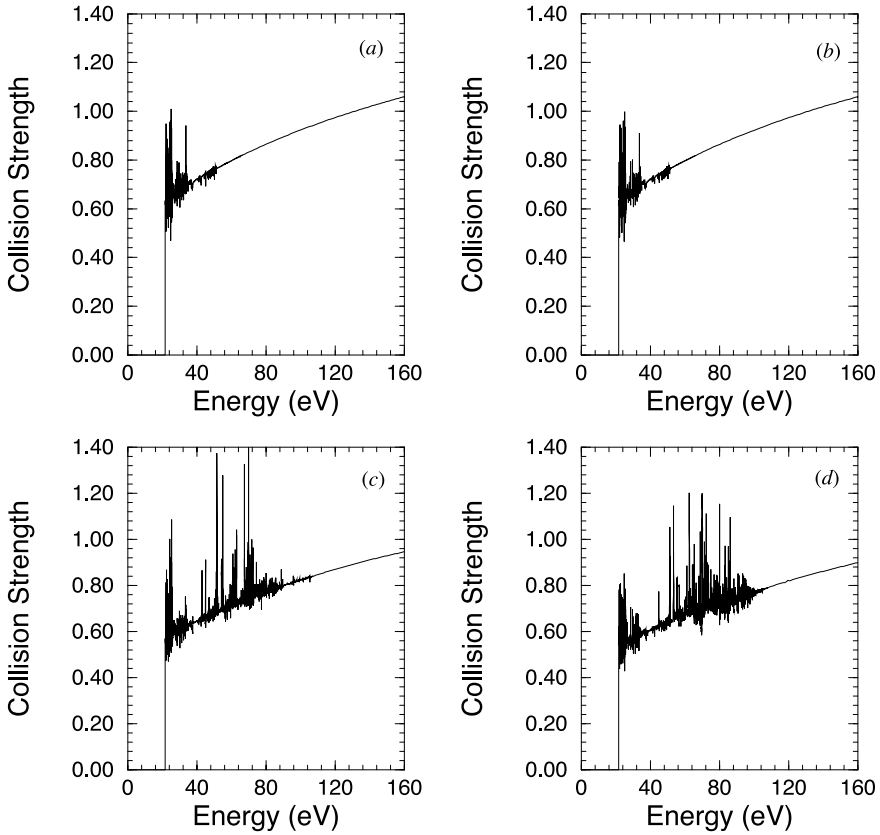

Figure 3. Collision strengths for excitation from $2s^2 2p^2\ ^3P_0$ to $2s2p^3\ ^3D_1$. (*a*) 20-level BP *R*-matrix calculation; (*b*) 20-level ICFT *R*-matrix calculation; (*c*) 62-level ICFT *R*-matrix calculation; (*d*) 138-level ICFT *R*-matrix calculation.

earlier calculations are quite different from the present ones. We noted in the description of these calculations [3] that the long-range multipole potentials were not included in the asymptotic part of the calculation. We have discovered from prior work that these have significant effects, especially on dipole-allowed transitions, even for high partial waves. In order to check on this, we performed an *LS R*-matrix calculation involving the 12-terms included in our 20-level ICFT calculation, both with and without the long-range multipole potentials. We found very large differences in the results. For example, at 5.0 Ryd, the value of the collision strength for the $2s^2 2p^2\ ^3P$–$2s2p^3\ ^3D$ transition was 7.395 with the long-range multipole potentials included, but only 5.186 with them turned off—this compares with the value from Aggarwal [4] of 5.137. In the case of the $2s^2 2p^2\ ^3P$–$2s2p^3\ ^3P$ transition at 5.0 Ryd, our collision strength with the long-range multipole potentials included was 6.592 compared with 5.099 without them, and the value from Aggarwal [4] was 4.626. Thus, it seems clear that one reason for the large differences between our results and those of these earlier calculations is the omission of the long-range multipole potentials from the earlier calculations.

However, we also made a 20-level ICFT calculation in which we excluded the long-range multipole potentials and transformed the unphysical *K*-matrices to pure pair coupling, rather than intermediate coupling; we still did not obtain good agreement with the effective collision

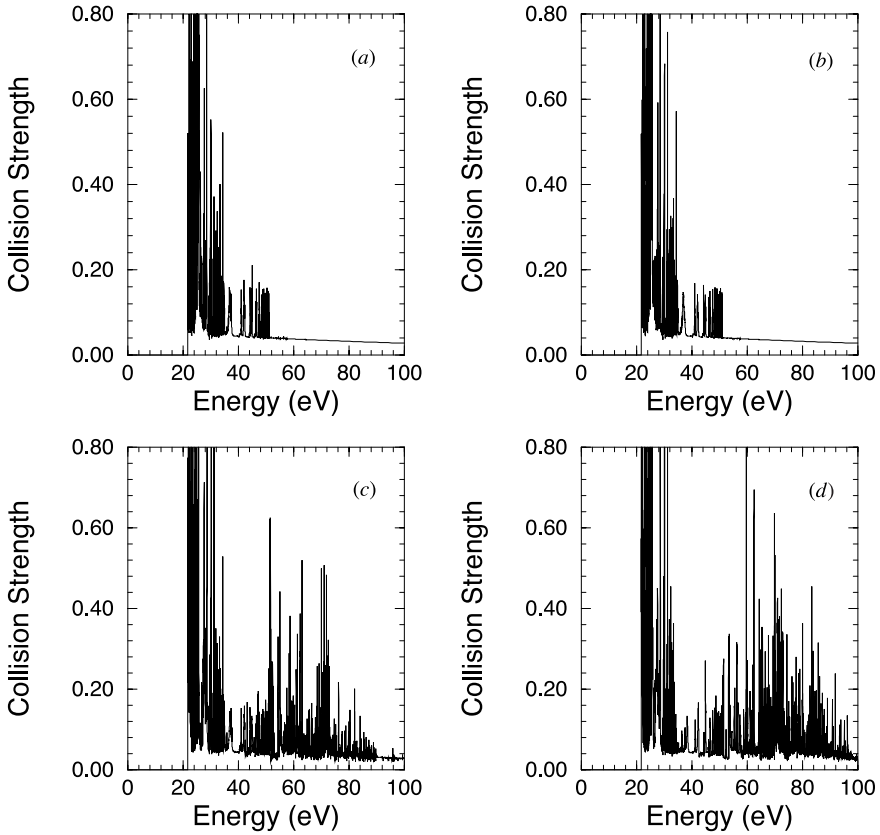

Figure 4. Collision strengths for excitation from $2s^22p^2\ ^3P_1$ to $2s2p^3\ ^3D_3$. (*a*) 20-level BP *R*-matrix calculation; (*b*) 20-level ICFT *R*-matrix calculation; (*c*) 62-level ICFT *R*-matrix calculation; (*d*) 138-level ICFT *R*-matrix calculation.

strengths of Aggarwal [5]. In fact, the differences are larger than the variations between our 20- and 138-level effective collision strengths for these transitions given in table 6. Thus we are unable to fully explain the source of these discrepancies with the earlier calculations.

In table 7, we compare the effective collision strengths calculated from the 62-level calculation with those determined from the 138-level calculation for transitions from the $2s^22p^2\ ^3P_0$ ground level to the levels of the $2s^22p3\ell$ configurations. Again, the additional states included in the 138-level calculation can both enhance and reduce the collision strength, depending on the transition. The difference between these two sets of collision strengths averaged over temperature varies from a low of 3.72% for the $2s^22p^2\ ^3P_0$–$2s^22p3p\ ^3D_1$ transition to a high of 32.1% for the $2s^22p^2\ ^3P_0$–$2s^22p3d\ ^3D_1$ transition; the average difference for all of the transitions given in table 7 is 13.3%.

It is important to note that we included the levels of $2s^22p4\ell$ configurations in the 138-level calculation in order to include the effects of coupling to these levels and the contribution from resonances attached to these levels. However, excitation collision strengths to these levels are not reliable since our calculation does not include configuration interaction between the levels of the $2s^22p4\ell$ configurations and the $2p^34\ell$ configurations, resonant contributions from higher Rydberg states or coupling to the higher Rydberg states and the continuum. For that reason, the effective collision strengths from our 138-level calculation, that are now available

Table 7. Ne^{4+} effective collision strengths for the transitions from the $2s^22p^2\ ^3P_0$ ground level to the levels of the $2s^22p3\ell$ configurations. For each transition, the first row is from the present 34-term, 62-level ICFT calculation and the second row is from the present 66-term, 138-level ICFT calculation.

	Electron temperature (K)						
Upper level	1.00×10^4	2.51×10^4	6.30×10^4	1.00×10^5	2.51×10^5	6.30×10^5	1.00×10^6
$2s^22p3s\ ^3P_0$	3.12×10^{-2}	3.15×10^{-2}	2.70×10^{-2}	2.27×10^{-2}	1.40×10^{-2}	7.77×10^{-3}	5.67×10^{-3}
	2.89×10^{-2}	2.74×10^{-2}	2.21×10^{-2}	1.83×10^{-2}	1.13×10^{-2}	6.50×10^{-3}	4.84×10^{-3}
$2s^22p3s\ ^3P_1$	1.47×10^{-1}	1.36×10^{-1}	1.10×10^{-1}	9.12×10^{-2}	5.73×10^{-2}	3.98×10^{-2}	3.86×10^{-2}
	1.24×10^{-1}	1.16×10^{-1}	9.42×10^{-2}	7.81×10^{-2}	5.04×10^{-2}	3.73×10^{-2}	3.68×10^{-2}
$2s^22p3s\ ^3P_2$	1.32×10^{-1}	1.23×10^{-1}	9.68×10^{-2}	7.76×10^{-2}	4.30×10^{-2}	2.12×10^{-2}	1.45×10^{-2}
	1.19×10^{-1}	1.08×10^{-1}	8.40×10^{-2}	6.74×10^{-2}	3.77×10^{-2}	1.88×10^{-2}	1.30×10^{-2}
$2s^22p3s\ ^1P_1$	8.19×10^{-2}	7.88×10^{-2}	6.04×10^{-2}	4.80×10^{-2}	2.69×10^{-2}	1.39×10^{-2}	1.00×10^{-2}
	6.50×10^{-2}	6.75×10^{-2}	5.13×10^{-2}	4.07×10^{-2}	2.31×10^{-2}	1.21×10^{-2}	8.68×10^{-3}
$2s^22p3p\ ^1P_1$	5.30×10^{-2}	4.42×10^{-2}	3.30×10^{-2}	2.73×10^{-2}	1.79×10^{-2}	1.14×10^{-2}	8.93×10^{-3}
	4.82×10^{-2}	4.01×10^{-2}	3.05×10^{-2}	2.56×10^{-2}	1.70×10^{-2}	1.07×10^{-2}	8.42×10^{-3}
$2s^22p3p\ ^3D_1$	5.65×10^{-2}	5.21×10^{-2}	4.04×10^{-2}	3.35×10^{-2}	2.19×10^{-2}	1.38×10^{-2}	1.08×10^{-2}
	6.07×10^{-2}	5.23×10^{-2}	3.96×10^{-2}	3.29×10^{-2}	2.13×10^{-2}	1.31×10^{-2}	1.01×10^{-2}
$2s^22p3p\ ^3D_2$	8.26×10^{-2}	6.74×10^{-2}	4.89×10^{-2}	3.97×10^{-2}	2.58×10^{-2}	1.84×10^{-2}	1.61×10^{-2}
	8.41×10^{-2}	6.73×10^{-2}	4.98×10^{-2}	4.13×10^{-2}	2.78×10^{-2}	2.02×10^{-2}	1.78×10^{-2}
$2s^22p3p\ ^3D_3$	7.56×10^{-2}	5.84×10^{-2}	4.00×10^{-2}	3.15×10^{-2}	1.86×10^{-2}	1.07×10^{-2}	8.05×10^{-3}
	5.62×10^{-2}	4.73×10^{-2}	3.53×10^{-2}	2.90×10^{-2}	1.79×10^{-2}	1.04×10^{-2}	7.84×10^{-3}
$2s^22p3p\ ^3S_1$	3.83×10^{-2}	3.15×10^{-2}	2.36×10^{-2}	1.93×10^{-2}	1.22×10^{-2}	7.52×10^{-3}	5.85×10^{-3}
	4.19×10^{-2}	3.43×10^{-2}	2.57×10^{-2}	2.11×10^{-2}	1.32×10^{-2}	7.81×10^{-3}	5.93×10^{-3}
$2s^22p3p\ ^3P_0$	1.02×10^{-1}	1.06×10^{-1}	1.00×10^{-1}	9.49×10^{-2}	8.73×10^{-2}	8.33×10^{-2}	7.98×10^{-2}
	7.57×10^{-2}	8.00×10^{-2}	7.64×10^{-2}	7.32×10^{-2}	6.92×10^{-2}	6.96×10^{-2}	6.84×10^{-2}
$2s^22p3p\ ^3P_1$	5.61×10^{-2}	5.72×10^{-2}	4.66×10^{-2}	3.94×10^{-2}	2.69×10^{-2}	1.79×10^{-2}	1.43×10^{-2}
	5.16×10^{-2}	5.05×10^{-2}	4.29×10^{-2}	3.69×10^{-2}	2.52×10^{-2}	1.64×10^{-2}	1.30×10^{-2}
$2s^22p3p\ ^3P_2$	3.78×10^{-2}	3.91×10^{-2}	3.05×10^{-2}	2.49×10^{-2}	1.59×10^{-2}	1.06×10^{-2}	8.70×10^{-3}
	4.36×10^{-2}	4.50×10^{-2}	3.70×10^{-2}	3.07×10^{-2}	1.94×10^{-2}	1.22×10^{-2}	9.93×10^{-3}
$2s^22p3p\ ^1D_2$	3.98×10^{-2}	3.89×10^{-2}	3.08×10^{-2}	2.62×10^{-2}	1.86×10^{-2}	1.27×10^{-2}	1.03×10^{-2}
	2.97×10^{-2}	3.00×10^{-2}	2.55×10^{-2}	2.22×10^{-2}	1.56×10^{-2}	1.05×10^{-2}	8.44×10^{-3}
$2s^22p3p\ ^1S_0$	8.98×10^{-3}	6.75×10^{-3}	4.79×10^{-3}	4.07×10^{-3}	3.00×10^{-3}	2.15×10^{-3}	1.76×10^{-3}
	6.65×10^{-3}	5.72×10^{-3}	4.41×10^{-3}	3.75×10^{-3}	2.50×10^{-3}	1.59×10^{-3}	1.26×10^{-3}
$2s^22p3d\ ^3F_2$	4.67×10^{-2}	3.79×10^{-2}	3.13×10^{-2}	2.85×10^{-2}	2.31×10^{-2}	1.69×10^{-2}	1.37×10^{-2}
	4.25×10^{-2}	3.84×10^{-2}	3.38×10^{-2}	3.10×10^{-2}	2.45×10^{-2}	1.75×10^{-2}	1.42×10^{-2}
$2s^22p3d\ ^1D_2$	3.16×10^{-2}	2.61×10^{-2}	2.18×10^{-2}	2.01×10^{-2}	1.66×10^{-2}	1.25×10^{-2}	1.03×10^{-2}
	2.80×10^{-2}	2.55×10^{-2}	2.25×10^{-2}	2.05×10^{-2}	1.61×10^{-2}	1.17×10^{-2}	9.60×10^{-3}
$2s^22p3d\ ^3F_3$	3.28×10^{-2}	2.46×10^{-2}	1.89×10^{-2}	1.70×10^{-2}	1.42×10^{-2}	1.24×10^{-2}	1.15×10^{-2}
	3.47×10^{-2}	3.10×10^{-2}	2.54×10^{-2}	2.25×10^{-2}	1.72×10^{-2}	1.36×10^{-2}	1.22×10^{-2}
$2s^22p3d\ ^3F_4$	2.38×10^{-2}	1.89×10^{-2}	1.52×10^{-2}	1.38×10^{-2}	1.12×10^{-2}	8.29×10^{-3}	6.81×10^{-3}
	2.04×10^{-2}	1.81×10^{-2}	1.61×10^{-2}	1.48×10^{-2}	1.18×10^{-2}	8.47×10^{-3}	6.90×10^{-3}
$2s^22p3d\ ^3D_1$	2.37×10^{-1}	2.35×10^{-1}	2.39×10^{-1}	2.48×10^{-1}	2.85×10^{-1}	3.66×10^{-1}	4.35×10^{-1}
	1.52×10^{-1}	1.58×10^{-1}	1.68×10^{-1}	1.78×10^{-1}	2.13×10^{-1}	2.90×10^{-1}	3.50×10^{-1}
$2s^22p3d\ ^3D_2$	3.85×10^{-2}	3.54×10^{-2}	3.25×10^{-2}	3.10×10^{-2}	2.70×10^{-2}	2.10×10^{-2}	1.75×10^{-2}
	3.35×10^{-2}	3.33×10^{-2}	3.02×10^{-2}	2.77×10^{-2}	2.22×10^{-2}	1.69×10^{-2}	1.43×10^{-2}
$2s^22p3d\ ^3D_3$	1.90×10^{-2}	1.78×10^{-2}	1.62×10^{-2}	1.55×10^{-2}	1.37×10^{-2}	1.14×10^{-2}	1.01×10^{-2}
	2.36×10^{-2}	2.21×10^{-2}	1.88×10^{-2}	1.67×10^{-2}	1.27×10^{-2}	9.79×10^{-3}	8.58×10^{-3}
$2s^22p3d\ ^3P_2$	1.49×10^{-2}	1.41×10^{-2}	1.30×10^{-2}	1.23×10^{-2}	1.03×10^{-2}	7.62×10^{-3}	6.23×10^{-3}
	2.12×10^{-2}	1.90×10^{-2}	1.67×10^{-2}	1.52×10^{-2}	1.15×10^{-2}	7.84×10^{-3}	6.24×10^{-3}
$2s^22p3d\ ^3P_1$	5.11×10^{-2}	5.05×10^{-2}	5.13×10^{-2}	5.30×10^{-2}	5.98×10^{-2}	7.50×10^{-2}	8.81×10^{-2}
	4.29×10^{-2}	4.10×10^{-2}	4.24×10^{-2}	4.43×10^{-2}	5.14×10^{-2}	6.63×10^{-2}	7.78×10^{-2}

Table 7. Continued.

	Electron temperature (K)						
Upper level	1.00×10^4	2.51×10^4	6.30×10^4	1.00×10^5	2.51×10^5	6.30×10^5	1.00×10^6
$2s^2 2p3d\ ^1P_1$	1.05×10^{-2}	1.01×10^{-2}	9.48×10^{-3}	9.10×10^{-3}	7.91×10^{-3}	6.07×10^{-3}	5.06×10^{-3}
	1.03×10^{-2}	1.02×10^{-2}	9.73×10^{-3}	9.06×10^{-3}	7.17×10^{-3}	5.13×10^{-3}	4.15×10^{-3}
$2s^2 2p3d\ ^3P_0$	3.24×10^{-3}	3.07×10^{-3}	2.89×10^{-3}	2.79×10^{-3}	2.47×10^{-3}	1.95×10^{-3}	1.65×10^{-3}
	4.28×10^{-3}	3.99×10^{-3}	3.59×10^{-3}	3.32×10^{-3}	2.70×10^{-3}	2.04×10^{-3}	1.71×10^{-3}
$2s^2 2p3d\ ^1F_3$	2.07×10^{-2}	2.02×10^{-2}	1.95×10^{-2}	1.89×10^{-2}	1.67×10^{-2}	1.30×10^{-2}	1.08×10^{-2}
	2.18×10^{-2}	2.08×10^{-2}	1.90×10^{-2}	1.76×10^{-2}	1.42×10^{-2}	1.06×10^{-2}	8.85×10^{-3}

on the internet at the CFADC site, are restricted to transitions between the lowest 49 levels up through the $2s^2 2p3d\ ^1F_3$ level.

3. Conclusions

We have made a series of *R*-matrix close-coupling calculations of electron-impact excitation in the C-like ion, Ne^{4+} with an increasing number of states in both the configuration-interaction expansion of the target and the close-coupling expansion. By comparing the results from these calculations, we have been able to demonstrate the combined effects on the effective collision strengths from a more complete target description, an increase in the size of the close-coupling expansion, and additional contributions from resonances attached to higher levels.

Our final 138-level calculation provides improved excitation data between levels of the $2s^2 2p^2$, $2s2p^3$ and $2p^4$ configurations as well as the first close-coupling data for excitation to the levels of the $2s^2 2p3\ell$ configurations. The electric-dipole radiative rates and the effective collision strengths between the lowest 49 levels, as determined from our largest calculation, are now available at the ORNL CFADC internet site.

Prior calculations on transitions within the $2s^2 2p^2$ ground configuration of Ne^{4+} appear to be reasonably accurate. However, the effective collision strengths from earlier calculations [5] for transitions between levels of the $2s^2 2p^2$ ground configuration and levels of the $2s2p^3$ excited configuration appear to include significant errors. Therefore, additional work is needed on other C-like ions in order to investigate the accuracy of prior data for excitation to levels of the $2s2p^3$ configuration and to add excitation data on transitions to the $2s^2 2p3\ell$ configurations.

Acknowledgments

DCG was supported by a US DoE Grant (DE-FG02-96-ER54367) with Rollins College and NRB was supported by a UK PPARC Grant (PPA/G/S/1997/00783) with the University of Strathclyde.

References

[1] Baluja K L, Burke P G and Kingston A E 1980 *J. Phys. B: At. Mol. Phys.* **13** 4675
[2] Aggarwal K M 1983 *J. Phys. B: At. Mol. Phys.* **16** 2405
[3] Aggarwal K M 1984 *Astrophys. J. Suppl.* **54** 1
[4] Aggarwal K M 1985 *Astrophys. J. Suppl.* **58** 289
[5] Aggarwal K M 1986 *Astrophys. J. Suppl.* **61** 699
[6] Lennon D J and Burke V M 1991 *Mon. Not. R. Astron. Soc.* **251** 628
[7] Lennon D J and Burke V M 1994 *Astron. Astrophys. Suppl. Ser.* **103** 273

[8] Griffin D C, Badnell N R and Pindzola M S 1998 *J. Phys. B: At. Mol. Opt. Phys.* **31** 3713
[9] Griffin D C, Badnell N R, Pindzola M S and Shaw J A 1999 *J. Phys. B: At. Mol. Opt. Phys.* **32** 2139
[10] Saraph H E 1972 *Comput. Phys. Commun.* **3** 256–68
Saraph H E 1978 *Comput. Phys. Commun.* **15** 247
[11] Froese Fischer C 1991 *Comput. Phys. Commun.* **64** 369
[12] Kelly R L 1987 *J. Phys. Chem. Ref. Data* **16** 149 Suppl. 1
[13] Aggarwal K M 1998 *Astrophys. J. Suppl.* **118** 589
[14] Seaton M J 1953 *Proc. R. Soc.* A **218** 400
[15] Burgess A and Tully J A 1992 *Astron. Astrophys.* **254** 436
[16] Berrington K A, Eissner W B and Norrington P H 1995 *Comput. Phys. Commun.* **92** 290
[17] Burke V M, Burke P G and Scott N J 1992 *Comput. Phys. Commun.* **69** 76
[18] Burgess A 1974 *J. Phys. B: At. Mol. Phys.* **7** L364
[19] Burgess A, Hummer D G and Tully J A 1970 *Phil. Trans. R. Soc.* A **266** 225
[20] Aggarwal K M, Deb N C, Keenan F P and Msezane A Z 2000 *J. Phys. B: At. Mol. Opt. Phys.* **33** L391
[21] Gorczyca T W, Robicheaux F, Pindzola M S, Griffin D C and Badnell N R 1995 *Phys. Rev.* A **52** 3877